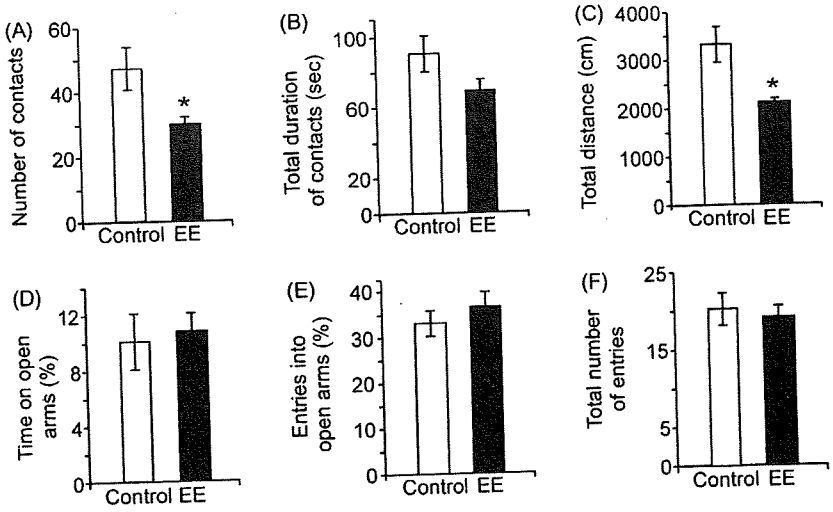

Fig. 3. Social interaction and emotional behavior in the elevated plus maze test in EE mice. The total number of contacts (A), total duration of contacts (B) an distance traveled (C) in the social interaction test are shown. Representative data of three independent batches of mice are shown (pairs of EE mice: $n=9$, pairs o control mice: $n=9$). The percentage of time spent in the open arms (D), the percentage of open arm entries (E) and the total number of arm entries (F) in the elevate plus maze test are shown. Representative data for three independent batches of mice are shown (EE: $n=18$, control: $n=18$). Data represent means ± S.E.M. $*p<0.05$

3.4. Newborn cells in the dentate gyri of EE mice

We examined newborn cells in the dentate gyri of EE mice by immunohistochemistry of BrdU labeling. Surviving BrdU-immunoreactive cells were observed in the dentate gyri of EE (Fig. 5A) and control mice (Fig. 5B) sacrificed four weeks after BrdU injection. To determine the phenotype of these BrdU-positive cells, we performed immunofluorescent labeling with BrdU and the neural marker NeuN (Fig. 5C), or the glial marker GFAP (Fig. 5D). We counted the double labeled cells with BrdU and NeuN or GFAP and found that environmental enrichment did not affect the differentiation of newly generated cells towards either a neuronal (EE, 90.6 ± 3.3% $n=3$; control, 89.0 ± 2.4%, $n=3$; $p=0.72$) or glial fate (EE 7.7 ± 1.7%, $n=3$; control, 6.4 ± 0.7%, $n=3$; $p=0.53$). Most sur viving BrdU-positive cells in the dentate gyri of mice housed i either environmental condition expressed NeuN, but not GFAI Quantitative analysis by counting the number of BrdU-labele cells confirmed an increase in the number of surviving BrdU positive cells in EE mice (Fig. 5E, EE: 548.5 ± 41.3, control 386.7 ± 60.2, $t(10)=3.64$, $p=0.005$). Moreover, the volumes o the dentate gyri of EE mice were similar to those of control mic (Fig. 5F, EE: 0.238 ± 0.009 mm^3, control: 0.227 ± 0.003 mm^3 $t(10)=1.16$, $p=0.27$), and the proliferation of newborn cell

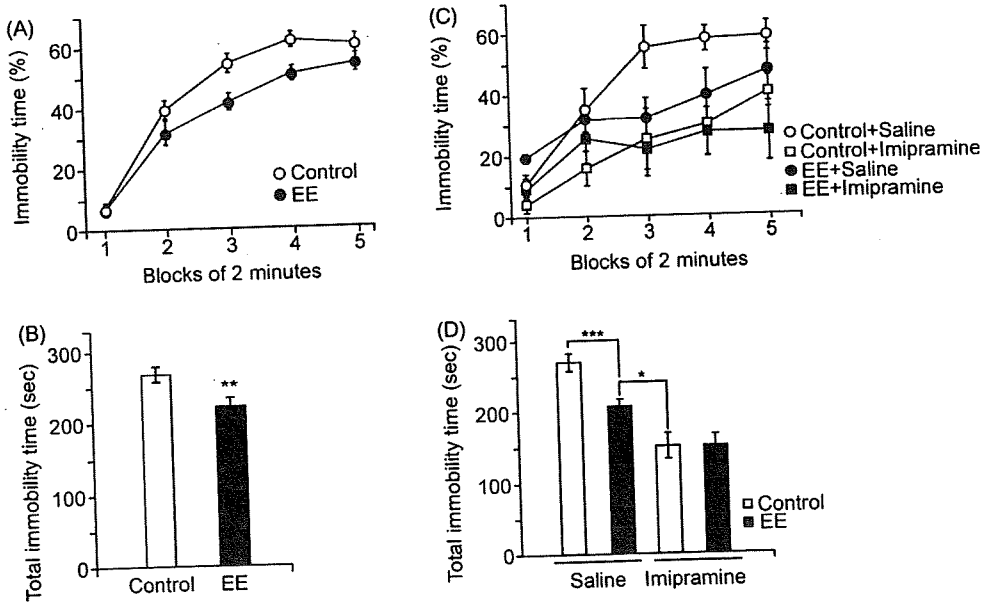

Fig. 4. Immobility time in the forced swim test in EE mice. Time courses of immobility time (A) and total immobility time during the test (B) in EE and contr mice (EE: $n=27$, control: $n=27$). (C) Effect of imipramine (10 mg/kg) on the time course of immobility time. Representative data for three independent batches mice are shown (EE + saline: $n=9$, control + saline: $n=9$, EE + imipramine: $n=9$, control + imipramine: $n=9$). (D) Total immobility time during the test in EE ar control mice administered with imipramine or saline. Results from three batches of mice are shown (EE + saline: $n=27$, control + saline: $n=27$, EE + imipramin $n=27$, control + imipramine: $n=27$). Data represent means ± S.E.M. $*p<0.05$, $**p<0.01$, $***p<0.001$.

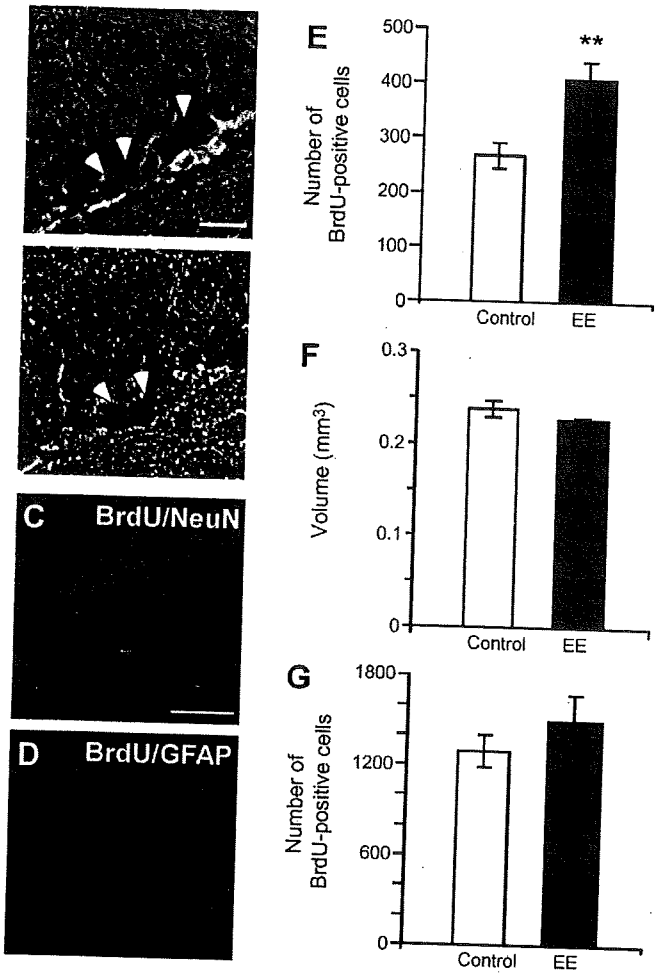

Fig. 5. Newborn cells in the dentate gyri of EE mice. Photomicrographs of BrdU-positive cells in the dentate gyrus of an EE (A) and a control (B) mouse, four weeks after BrdU injection (survival paradigm), are shown. Arrow heads indicate BrdU-positive cells. Scale bar = 25 μm. Surviving cells were double-labeled with BrdU and NeuN (C) or GFAP (D). Merged images are shown. Scale bar = 50 μm. (E) The number of BrdU-positive cells in the survival paradigm (EE: $n = 6$, control: $n = 6$). (F) The volume of dentate gyri in the survival paradigm (EE: $n = 6$, control: $n = 6$). (G) The number of BrdU-positive cells in the proliferation paradigm (EE: $n = 11$, control: $n = 7$). Data represent means ± S.E.M. $^{**}p < 0.01$.

in the dentate gyri of mice sacrificed one day after BrdU injection was not significantly changed by environmental enrichment (Fig. 5G, EE: 1300.9 ± 158.2, control: 1094.6 ± 121.5, $t(16) = 0.93$, $p = 0.37$).

4. Discussion

Our results support the hypothesis that environmental enrichment during adulthood has beneficial effects on behaviors in mice. The distance traveled by EE mice was shorter than that traveled by control mice (Fig. 1A and B), indicating a reduction in locomotor activity in a novel environment during an open field test, as previously reported [2,21,40]. EE mice showed a longer latency to fall off in a wire hang test (Table 1) and a reduction in total immobility time in a forced swim test (Fig. 4A and B). These results suggest that the decrease in locomotor activity is not due to loss of motor function. In addition, locomotor activity was not significantly different between two groups within a few minutes of the start of recording; however, the activity gradually became lower in EE mice (Fig. 1A). This reduction in locomotor activity in EE mice could be a result of a quick habituation to a novel environment. One reason for this might be that EE mice had been exposed to changing stimuli in their housing environment (i.e., several toys and wide cage).

Our results showed that EE mice spent more time in the center of the open field apparatus (Fig. 1C), a behavior that is thought to reflect reduced anxiety [7]. However, in this study, environmental enrichment failed to improve the anxiety-like behavior observed in the elevated plus maze (Fig. 3D–F). This is in disagreement with results obtained in mice housed in EEs from an early age or over a longer period [1,19]. As the degree of conflict might be more in the elevated plus maze test than in free-exploration in the open field test [6,7], our EE paradigm might be insufficient to reduce the anxiety in more conflictive situations. In this study, EE mice showed a significant decrease in the number of social contacts (Fig. 3A–C); however, it is likely that this decrease is a consequence of the decreased locomotor activity in EE mice. The total duration of social contacts was not significantly different between the two groups. Thus, it is unlikely that EE mice are less social. The results of the social interaction test (Fig. 3A–C) and startle response test (Fig. 2A) also disagreed with those in mice housed in EEs from an early age and/or over a longer period [31,40]. The nature of EE protocols varies widely between laboratories; however, the timing and duration of environmental enrichment might be important parameters for the effects on behaviors [33]. In addition, there was no significant difference in PPI between EE and control mice (Fig. 2B), suggesting that exposure to an EE during adulthood did not affect sensory motor gating, at least in our paradigm. The forced swim test is known to assess "behavioral despair" in rodents by the measurement of immobility time [34]. Reduced immobility time in the forced swim test was found in EE mice (Fig. 4). We confirmed in a preliminary experiment that imipramine did not affect motor activity (data not shown). It is unlikely that this phenomenon is due to the hyperactivity of the EE mice, as they showed decreased locomotor activity in the open field test (Fig. 1A and B). Thus, it suggests that the EE enhanced the tolerance against an inescapable, stressful situation. The beneficial effect of environmental enrichment on depression-related behavior was also shown in rats reared in an EE during the first month of life [24]. Our result showed that this effect could be also achieved in mice housed in an EE during adulthood. Experience-dependent plasticity is induced by EE [33]; thus, EE might also induce an alteration in depression-related behavior in adult rodents.

The enhanced neurogenesis in adult animals housed in an EE is thought to be a potential mechanism mediating the behavioral effects of EEs [20,33,38]. We found enhanced survival of newborn cells in the dentate gyri of EE mice (Fig. 5A, B and E), as reported previously [20]. As the volume of the dentate gyrus was similar between control and EE mice (Fig. 5F), the enhanced survival of newborn cells might not be affected by the volume of the dentate gyrus. Our results show that EE can affect depression-related behavior, and that EE enhances the

survival of newly generated cells, most of which differentiate into neurons, consistent with a previous study [20]. However, it was impossible to show a direct relationship between the altered behaviors and the increase in newborn cells induced by an EE. In a recent study, the reduction in adult-generated cells in the dentate gyrus due to methylazoxymethanol acetate, a toxin that inhibits cell proliferation, prevents the EE-induced improvement in hippocampal-dependent memory [4], suggesting that EE-induced neurogenesis may have an important role in behavioral outputs. On the other hand, the arrest of adult hippocampal neurogenesis does not attenuate the effect of EE on spatial learning and anxiety-like behavior [28]. An investigation into a causal relationship between increased neurogenesis and the behavioral effects of EEs is underway. Exposure to an EE increases the gene expression of several growth factors and neurotransmitters [38]. The effects of environmental enrichment can be achieved through multiple pathways, including neurogenesis-independent mechanisms. Further studies are necessary to understand the mechanism underlying the effects of environmental enrichment.

Acknowledgements

This work was supported by Grants-in-Aid from the Japanese Ministry of Health, Labor and Welfare, the Japanese Ministry of Education, Culture, Sports, Science and Technology, and Japan Foundation for Neuroscience and Mental Health.

References

[1] Benaroya-Milshtein N, Hollander N, Apter A, Kukulansky T, Raz N, Wilf A, et al. Environmental enrichment in mice decreases anxiety, attenuates stress responses and enhances natural killer cell activity. Eur J Neurosci 2004;20:1341–7.
[2] Bezard E, Dovero S, Belin D, Duconger S, Jackson-Lewis V, Przedborski S, et al. Enriched environment confers resistance to 1-methyl-4-phenyl-1,2,3,6-tetrahydropyridine and cocaine: involvement of dopamine transporter and trophic factors. J Neurosci 2003;23:10999–1007.
[3] Bremner JD, Narayan M, Anderson ER, Staib LH, Miller HL, Charney DS. Hippocampal volume reduction in major depression. Am J Psychiatry 2000;157:115–8.
[4] Bruel-Jungerman E, Laroche S, Rampon C. New neurons in the dentate gyrus are involved in the expression of enhanced long-term memory following environmental enrichment. Eur J Neurosci 2005;21:513–21.
[5] Cameron HA, McKay RD. Adult neurogenesis produces a large pool of new granule cells in the dentate gyrus. J Comp Neurol 2001;435:406–17.
[6] Chapillon P, Manneche C, Belzung C, Caston J. Rearing environmental enrichment in two inbred strains of mice. 1. Effects on emotional reactivity. Behav Genet 1999;29:41–6.
[7] Crawley JN. What's wrong with my mouse? New York: Wiley-Liss; 2000.
[8] Cryan JF, Markou A, Lucki I. Assessing antidepressant activity in rodents: recent developments and future needs. Trends Pharmacol Sci 2002;23:238–45.
[9] Cryan JF, Mombereau C. In search of a depressed mouse: utility of models for studying depression-related behavior in genetically modified mice. Mol Psychiatry 2004;9:326–57.
[10] Cryan JF, Valentino RJ, Lucki I. Assessing substrates underlying the behavioral effects of antidepressants using the modified rat forced swimming test. Neurosci Biobehav Rev 2005;29:547–69.
[11] Duffy SN, Craddock KJ, Abel T, Nguyen PV. Environmental enrichment modifies the PKA-dependence of hippocampal LTP and improves hippocampus-dependent memory. Learn Mem 2001;8:26–34.
[12] Duman RS. Depression: a case of neuronal life and death? Biol Psychiatry 2004;56:140–5.
[13] Eriksson PS, Perfilieva E, Bjork-Eriksson T, Alborn AM, Nordborg C, Peterson DA, et al. Neurogenesis in the adult human hippocampus. Nat Med 1998;4:1313–7.
[14] File SE. The use of social interaction as a method for detecting anxiolytic activity of chlordiazepoxide-like drugs. J Neurosci Methods 1980;2:219–38.
[15] Gould E, Tanapat P. Stress and hippocampal neurogenesis. Biol Psychiatry 1999;46:1472–9.
[16] Hashimoto R, Nakamura Y, Komai S, Kashiwagi Y, Tamura K, Goto T, et al. Site-specific phosphorylation of neurofilament-L is mediated by calcium/calmodulin-dependent protein kinase II in the apical dendrites during long-term potentiation. J Neurochem 2000;75:373–82.
[17] Hashimoto R, Nakamura Y, Imamura K, Nakadate K, Kashiwagi Y, Matsumoto N, et al. Visual stimulation-induced phosphorylation of neurofilament-L in the visual cortex of dark-reared rats. Eur J Neurosci 2001;14:1237–45.
[18] Hastings NB, Gould E. Rapid extension of axons into the CA3 region by adult-generated granule cells. J Comp Neurol 1999;413:146–54.
[19] Hellemans KG, Benge LC, Olmstead MC. Adolescent enrichment partially reverses the social isolation syndrome. Brain Res Dev Brain Res 2004;150:103–15.
[20] Kempermann G, Kuhn HG, Gage FH. More hippocampal neurons in adult mice living in an enriched environment. Nature 1997;386:493–5.
[21] Kempermann G, Gast D, Gage FH. Neuroplasticity in old age: sustained fivefold induction of hippocampal neurogenesis by long-term environmental enrichment. Ann Neurol 2002;52:135–43.
[22] Kessler RC. The effects of stressful life events on depression. Annu Rev Psychol 1997;48:191–214.
[23] Madsen TM, Treschow A, Bengzon J, Bolwig TG, Lindvall O, Tingstrom A. Increased neurogenesis in a model of electroconvulsive therapy. Biol Psychiatry 2000;47:1043–9.
[24] Magalhaes A, Summavielle T, Tavares MA, de Sousa L. Effects of postnatal cocaine exposure and environmental enrichment on rat behavior in a forced swim test. Ann N Y Acad Sci 2004;1025:619–29.
[25] Malberg JE, Eisch AJ, Nestler EJ, Duman RS. Chronic antidepressant treatment increases neurogenesis in adult rat hippocampus. J Neurosci 2000;20:9104–10.
[26] Manji HK, Drevets WC, Charney DS. The cellular neurobiology of depression. Nat Med 2001;7:541–7.
[27] McEwen BS. Stress and hippocampal plasticity. Annu Rev Neurosci 1999;22:105–22.
[28] Meshi D, Drew MR, Saxe M, Ansorge MS, David D, Santarelli L, et al. Hippocampal neurogenesis is not required for behavioral effects of environmental enrichment. Nat Neurosci 2006;9:729–31.
[29] Miyakawa T, Yamada M, Duttaroy A, Wess J. Hyperactivity and intact hippocampus-dependent learning in mice lacking the M1 muscarinic acetylcholine receptor. J Neurosci 2001;21:5239–50.
[30] Miyakawa T, Leiter LM, Gerber DJ, Gainetdinov RR, Sotnikova TD, Zeng H, et al. Conditional calcineurin knockout mice exhibit multiple abnormal behaviors related to schizophrenia. Proc Natl Acad Sci USA 2003;100:8987–92.
[31] Morley-Fletcher S, Rea M, Maccari S, Laviola G. Environmental enrichment during adolescence reverses the effects of prenatal stress on play behaviour and HPA axis reactivity in rats. Eur J Neurosci 2003;18:3367–74.
[32] Nestler EJ, Barrot M, DiLeone RJ, Eisch AJ, Gold SJ, Monteggia LM. Neurobiology of depression. Neuron 2002;34:13–25.
[33] Nithianantharajah J, Hannan AJ. Enriched environments, experience-dependent plasticity and disorders of the nervous system. Nat Rev Neurosci 2006;7:697–709.
[34] Porsolt RD, Le Pichon M, Jalfre M. Depression: a new animal model sensitive to antidepressant treatments. Nature 1977;266:730–2.
[35] Santarelli L, Saxe M, Gross C, Surget A, Battaglia F, Dulawa S, et al. Requirement of hippocampal neurogenesis for the behavioral effects of antidepressants. Science 2003;301:805–9.

[36] Sheline YI, Wang PW, Gado MH, Csernansky JG, Vannier MW. Hippocampal atrophy in recurrent major depression. Proc Natl Acad Sci USA 1996;93:3908–13.
[37] Shors TJ, Miesegaes G, Beylin A, Zhao M, Rydel T, Gould E. Neurogenesis in the adult is involved in the formation of trace memories. Nature 2001;410:372–6.
[38] van Praag H, Kempermann G, Gage FH. Neural consequences of environmental enrichment. Nat Rev Neurosci 2000;1:191–8.
[39] van Praag H, Schinder AF, Christie BR, Toni N, Palmer TD, Gage FH. Functional neurogenesis in the adult hippocampus. Nature 2002;415:1030–4.
[40] Varty GB, Paulus MP, Braff DL, Geyer MA. Environmental enrichment and isolation rearing in the rat: effects on locomotor behavior and startle response plasticity. Biol Psychiatry 2000;47:864–73.
[41] Wong ML, Licinio J. Research and treatment approaches to depression. Nat Rev Neurosci 2001;2:343–51.
[42] Young D, Lawlor PA, Leone P, Dragunow M, During MJ. Environmental enrichment inhibits spontaneous apoptosis, prevents seizures and is neuroprotective. Nat Med 1999;5:448–53.

Available online at www.sciencedirect.com
ScienceDirect
Bioorganic & Medicinal Chemistry 15 (2007) 6810–6818
Bioorganic & Medicinal Chemistry

Identification of novel chemical inhibitors for ubiquitin C-terminal hydrolase-L3 by virtual screening

Kazunori Hirayama,[a,b] Shunsuke Aoki,[b,*] Kaori Nishikawa,[b] Takashi Matsumoto[a] and Keiji Wada[b]

[a]*Department of Electrical Engineering and Bioscience, Graduate School of Advanced Science and Engineering, Waseda University, 3-4-1 Okubo, Shinjuku-ku, Tokyo 169-8555, Japan*
[b]*Department of Degenerative Neurological Diseases, National Institute of Neuroscience, National Center of Neurology and Psychiatry, 4-1-1 Ogawa-Higashi, Kodaira, Tokyo 187-8502, Japan*

Received 11 May 2007; revised 14 July 2007; accepted 18 July 2007
Available online 19 August 2007

Abstract—UCH-L3 (ubiquitin C-terminal hydrolase-L3) is a de-ubiquitinating enzyme that is a component of the ubiquitin–proteasome system and known to be involved in programmed cell death. A previous study of high-throughput drug screening identified an isatin derivative as a UCH-L3 inhibitor. In this study, we attempted to identify a novel inhibitor with a different structural basis. We performed in silico structure-based drug design (SBDD) using human UCH-L3 crystal structure data (PDB code; 1XD3) and the virtual compound library (ChemBridge CNS-Set), which includes 32,799 chemicals. By a two-step virtual screening method using DOCK software (first screening) and GOLD software (second screening), we identified 10 compounds with GOLD scores of over 60. To address whether these compounds exhibit an inhibitory effect on the de-ubiquitinating activity of UCH-L3, we performed an enzymatic assay using ubiquitin-7-amido-4-methylcoumarin (Ub-AMC) as the substrate. As a result, we identified three compounds with similar basic dihydro-pyrrole skeletons as UCH-L3 inhibitors. These novel compounds may be useful for the research of UCH-L3 function, and in drug development for UCH-L3-associated diseases.

1. Introduction

The ubiquitin–proteasome system is responsible for the regulation of cellular proteolysis. In this system, ubiquitination serves as a targeting signal for proteolysis.[1] Ubiquitin C-terminal hydrolase-L3 (UCH-L3) is one of the components of the ubiquitin–proteasome system and hydrolyzes ubiquitin C-terminal adducts for the recycling of cellular ubiquitin.[2] Ubiquitin with C-terminal adducts is a substrate for UCH-L3, and ubiquitin with a free C-terminus is recycled within the ubiquitin–proteasome system. There is some evidence that UCH-L3 plays an important role in programmed cell death. Programmed cell death is implicated in a number of human diseases, including neurodegenerative disease,[3] autoimmune disease,[4] cancers[5,6], etc. Loss of UCH-L3 leads to programmed cell death by apoptosis of certain type of cells in vivo, germ line cells and photoreceptor cells.[7,8] High-level expression of UCH-L3 genes and proteins, and acceleration of UCH-L3 enzymatic activity is reported in multiple types of cancer cells,[5,6] suggesting that UCH-L3 activity may be required for cancer cell survival. Therefore, UCH-L3 is a potential target for drug development to control programmed cell death in specific types of cells including cancer cells.

Structure-based drug design (SBDD) is a method used to discover novel leads for drug development as it enables more rapid hit identification than the classical screening methods of in vitro or in vivo biological assays. The computer-based approach for drug screening, using molecular docking, is a shortcut method when the crystal structure of a target protein is available. Key methodologies for docking small molecules to protein were developed during the early 1980s,[9] and various types of docking simulation software are now available, for example, DOCK,[10] GOLD, and FlexX.[11] BCR-ABL tyrosine kinase inhibitors (IC_{50} values ranging from 10 to 200 μM) were successfully

Keywords: UCH-L3; Dihydro-pyrrole; Structure-based drug design; Virtual screening.
* Corresponding author. Tel.: +81 42 341 2712x5144; fax: +81 42 346 1745; e-mail: aokis@ncnp.go.jp

0968-0896/$ - see front matter © 2007 Elsevier Ltd. All rights reserved.
doi:10.1016/j.bmc.2007.07.016

identified by virtual screening of 200,000 compounds against crystal structures using DOCK,[12] implemented by the anchor-and-grow algorithm with respect to ligand flexibility.[10] Human thymidine phosphorylase inhibitor (IC_{50} = 77 μM) was also identified by virtual screening of 250,521 compounds using DOCK.[13] Furthermore, metallo-β-lactamase inhibitors (IC_{50} values less than 15 μM) were identified through virtual screening by GOLD,[14] using the genetic algorithm for ligand flexibility.

The advantage of chaining different docking programs was evaluated and the results suggested that virtual ligand screening is performed faster with reasonable accuracy by using chained screening, than by using a single program with default parameters.[15] In this study, the results of chained docking against UCH-L3 crystal structure were examined by UCH-L3 hydrolysis activity assay to validate the efficacy of the DOCK–GOLD SBDD method. We identified three inhibitors (IC_{50} = 100–150 μM) of UCH-L3 by the DOCK–GOLD virtual screening of 32,799 compounds.

2. Results and discussion

2.1. Protein preparation and chemical database

In the 3D structure of the UCH-L3-ubiquitin complex, ubiquitin C-terminus is buried in the active site cleft among four active site residues of UCH-L3: Gln89, Cys95, His169, and Asp184.[16,17] During the virtual screening process by DOCK and GOLD, the protein–ligand interacting site was restricted to the binding site of the three ubiquitin C-terminal amino residues (as described in Section 4), in order that the outcome could be verified by a ubiquitin C-terminal hydrolase enzymatic assay. The first DOCK screening was performed against 32,799 compounds of CNS-Set, which was prefiltered by RPBS under the most modest filtering condition.[18]

2.2. DOCK and GOLD screenings

To screen for compounds that bind to the active site, the first screening was performed by DOCK, and the protein–ligand interaction area was restricted to the ubiquitin binding site of UCH-L3 (see Section 4). The top-scoring 1780 compounds (5.4% of the initial 32,799 compounds) with energy scores of less than −30 kcal/mol were selected for further screening. These compounds were then re-screened by GOLD twice, with different genetic algorithm (GA) settings. To predict binding ability to the active site cleft accurately, the protein–ligand interacting area was defined in approximately the same way as in the first DOCK screening step (see Section 4). Screening by GOLD consisted of two rounds. Using the GOLD score, we initially extracted the top scoring 100 compounds from 1780 compounds, using the 7–8 times speed-up GA parameter settings. These 100 compounds were then re-scored using the default GA settings (see Section 4) to more accurately predict binding ability. Ten compounds with GOLD scores of over 60 were predicted to bind to the UCH-L3 active site; that is, 0.03% of the total number of chemical compounds was screened.

2.3. IC_{50} determination

A previous study demonstrated that compounds with GOLD scores of about 60 may inhibit enzyme activity with IC_{50} values of 10–100 μM.[19] An enzyme assay was performed among the top 10 chemicals to address whether they actually bind to the UCH-L3 active site with the predicted affinities (Table 1 and Fig. 1).

Ubiquitin-7-amido-4-methylcoumarin (Ub-AMC; AMC attaches to the carboxyl terminus of ubiquitin) is a fluorogenic substrate of UCH-L3 and other UCH isozymes. UCH-L3 is known to hydrolyze Ub-AMC into free ubiquitin and AMC,[20,21] and the hydrolyzed AMC group is excited at light wavelength of 355 nm and emits fluorescence at 460 nm. Hydrolysis activity of UCH-L3 is inhibited if a compound binds to its active site and thus blocks interaction between the active site of UCH-L3 and the ubiquitin C-terminus. Inhibition of hydrolysis of Ub-AMC leads to a lower concentration of free AMC and hence a lower level of fluorescence intensity.

We experimentally determined the affinity constant (K_m) of Ub-AMC hydrolysis by human UCH-L3 as 83.3 ± 1.5 nM (mean ± SEM, from three independent experiments). The candidate compounds identified by

Table 1. GOLD scores of the top 10 ranked chemicals after GOLD calculation[a]

Docking rank/Compound No.	Compound name	GOLD scores
1	1-Benzyl-3-hydroxy-4-(5-methyl-2-furoyl)-5-(3-pyridinyl)-1,5-dihydro-2*H*-pyrrol-2-one	66.01
2	3-[4-Methyl-5-({[3-(2-thienyl)-1,2,4-oxadiazol-5-yl]methyl}thio)-4*H*-1,2,4-triazol-3-yl]-1*H*-indole	65.62
3	*N*-{4-[1-(2-Furoyl)-5-(2-furyl)-4,5-dihydro-1*H*-pyrazol-3-yl]phenyl}methanesulfonamide	64.85
4	N^1-Cyclopropyl-N^2-(4-methoxyphenyl)-N^2-[(4-methylphenyl)sulfonyl]glycinamide	64.76
5	*N*-{3-[1-Acetyl-5-(2-thienyl)-4,5-dihydro-1*H*-pyrazol-3-yl]phenyl}ethanesulfonamide	64.23
6	3-Hydroxy-5-(4-methoxyphenyl)-1-(1,3,4-thiadiazol-2-yl)-4-(2-thienylcarbonyl)-1,5-dihydro-2*H*-pyrrol-2-one	62.96
7	5-(4-Fluorophenyl)-3-hydroxy-4-(5-methyl-2-furoyl)-1-(3-pyridinylmethyl)-1,5-dihydro-2*H*-pyrrol-2-one	62.73
8	N^1-Cyclopropyl-N^2-[(4-methoxyphenyl)sulfonyl]-N^2-(4-methylphenyl)glycinamide	62.52
9	N^1-Cyclopentyl-N^2-(3-methoxyphenyl)-N^2-(phenylsulfonyl)glycinamide	62.39
10	4-({[5-(2-Furyl)-4-phenyl-4*H*-1,2,4-triazol-3-yl]thio}methyl)-1,3-thiazol-2-amine	62.35

[a] Ten compounds are listed according to the top 10 rank of GOLD scores and assigned the number corresponding to GOLD score ranks.

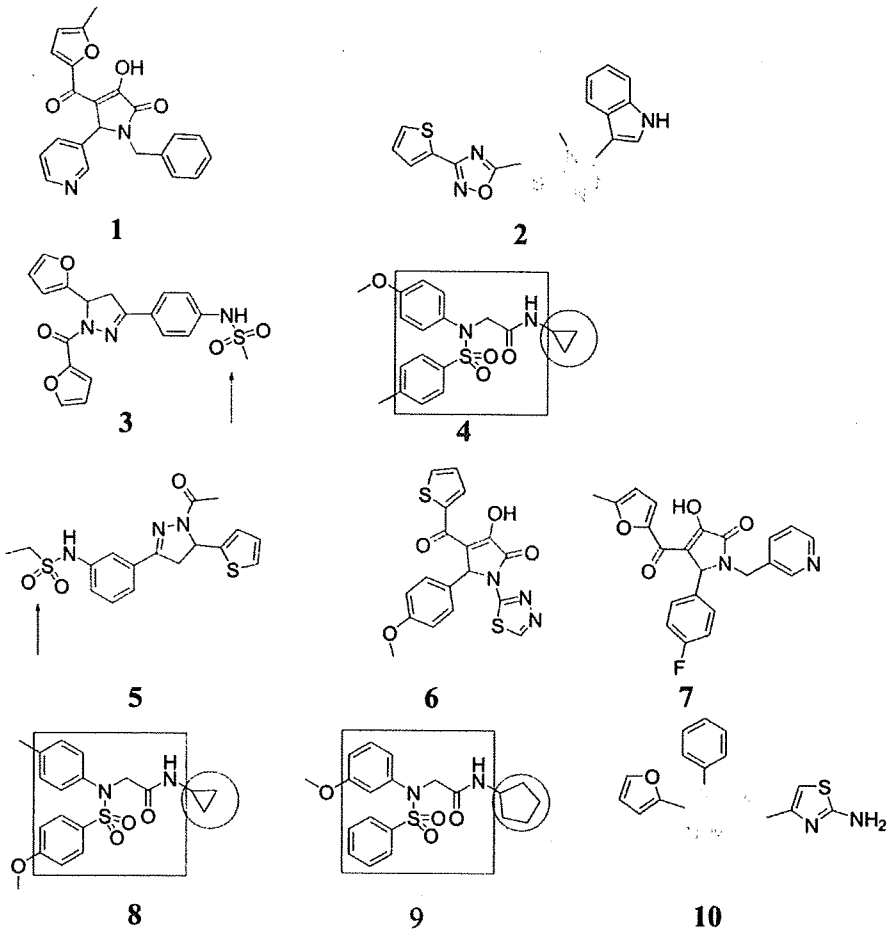

Figure 1. Top 10 ranked compounds identified by DOCK and GOLD screening. Note that there are several shared basic skeletons and functional groups: 1,5-dihydro-2*H*-pyrrol-2-one (drawn in red, compounds **1**, **6**, and **7**), glycinamide (boxed in red, compounds **4**, **8**, and **9**), cycloalkane group (circled in red, compounds **4** and **8**; cyclopropyl, compound **9**; cyclopentyl), 4,5-dihydro-1*H*-pyrazol-3-yl phenyl (drawn in blue, compounds **3** and **5**), sulfonamide (pointed, compounds **3** and **5**), and 4*H*-1,2,4-triazol-3-yl (drawn in green, compounds **2** and **10**).

DOCK–GOLD chained docking screening were tested for their ability to inhibit the hydrolysis activity of UCH-L3, at the Ub-AMC concentration equivalent to the K_m value. Four compounds among these candidates inhibited enzyme activity (Fig. 2a). We did not test the inhibitory effects of compound **3**, as it is a fluorogenic chemical with an emission wavelength of 460 nm. Compounds **1**, **6**, and **7** significantly inhibited the hydrolysis activity of UCH-L3 (initial velocity of Ub-AMC hydrolysis; nM/s [Fig. 2b]). Compounds **1** (401 μM), **6** (375 μM), and **7** (350 μM) inhibited the hydrolysis activity by 83.2 ± 1.5%, 76.5 ± 0.6%, and 76.8 ± 1.0%, respectively, as compared with control DMSO ($p < 0.01$, vs control; Dunnett's test). The IC_{50} value of compound **2** should hypothetically be several hundred μM. Although compound **2** (380 μM) inhibited hydrolysis activity by 16.2 ± 2.1% as compared with control DMSO, the difference was not found to be significant by Dunnett's test. Five other compounds were unable to inhibit the UCH-L3 hydrolysis activity: compound **4** (334 μM; final concentration), compound **5** (331 μM), compound **8** (401 μM), compound **9** (386 μM), and compound **10** (387 μM) (Fig. 2b). Experimentally determined IC_{50} values of compounds **1**, **6**, and **7** (Fig. 3) were as follows: compound **1** (103 μM), compound **6** (154 μM), and compound **7** (123 μM).

2.4. Competitive inhibitor

To show that the identified compounds bind to the active site of the UCH-L3, various concentrations of compound **1** and iodoacetamide (108 mM) were added to UCH-L3/Ub-AMC reaction buffer. Iodoacetamide is a non-competitive inhibitor of UCH-L3 (Fig. 4a). It is a thiol alkylating agent of the UCH-L family and derivatizes and inactivates the active site leading to loss of UCH-L3 enzymatic activity.[22] In the presence of compound **1** and iodoacetamide, the percentage of active UCH-L3 reduced by iodoacetamide treatment was recovered in comparison with the control, and the recovery was dependent on the concentration of compound **1** (Fig. 4b). Our results showed that compound **1** is a competitive inhibitor of UCH-L3. This suggests that compound **1** bound to the UCH-L3 active site to prevent iodoacetamide from inactivating it.

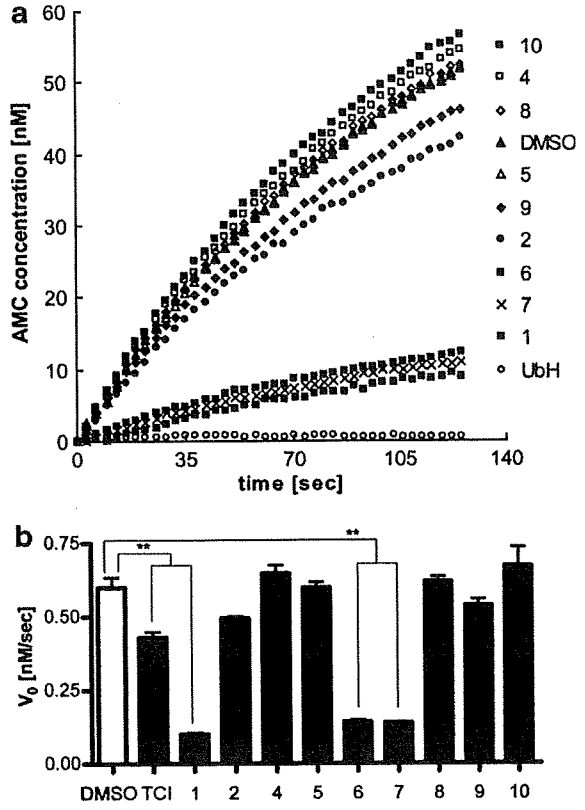

Figure 2. Analysis of UCH-L3 inhibitory effects of compounds 1–10. (a) Kinetics of UCH-L3-catalyzed hydrolysis of Ub-AMC with the compounds. Fluorescence intensity was converted to AMC concentration by subtracting the intensity of fully hydrolyzed substrate from that of solution without substrate. Concentrations of compounds are as follows: compound **1** (401 μM); compound **2** (380 μM); compound **4** (334 μM); compound **5** (331 μM); compound **6** (375 μM); compound **7** (350 μM); compound **8** (401 μM); compound **9** (386 μM); and compound **10** (387 μM). As a known inhibitor, ubiquitin-aldehyde (Ub-H, 120 nM) was used. Each value represents the mean of three independent experiments. (b) Inhibitory effects of compounds on initial velocity of hydrolysis (V_0) are shown. Fluorescence intensity was converted by the same method described in (a). 4,5,6,7-Tetrachloroindan-1,3-dione (TCI, 20 μM) was used as a UCH-L3 selective inhibitor with IC_{50} of 600 nM.[22] Each value represents the mean ± SEM of three independent experiments. Dunnett's multiple comparison test was performed using GraphPad Prism software (**: $p < 0.01$, DMSO as control).[29]

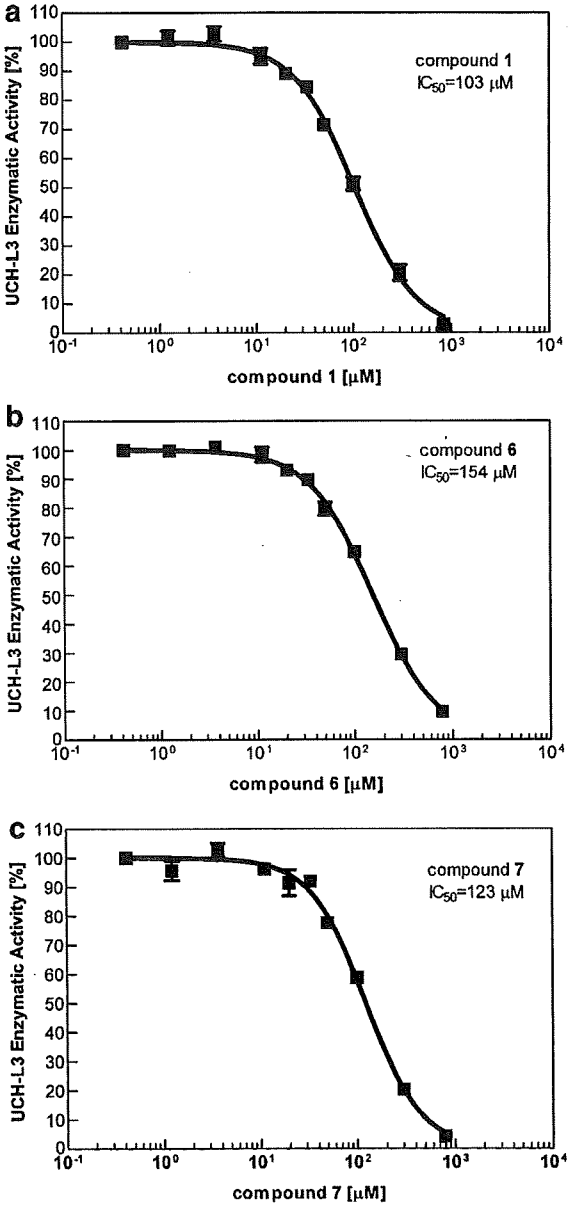

Figure 3. IC_{50} curves of compounds for UCH-L3 enzymatic activity. (a) Compound **1**, (b) compound **6**, and (c) compound **7**. The horizontal axis shows the concentration of each compound. The vertical axis shows the relative UCH-L3 enzymatic activity [%] in comparison with maximal initial velocity. IC_{50} values are shown in graphs. Each plotted value represents the mean ± SEM of three independent experiments.

In order to show that the compounds **1**, **6**, and **7** bind to UCH-L3, Biacore 100 analysis was conducted. Biacore 100 analysis detects interaction between a small molecule and protein and enables quantification of the interaction.[23] The results showed that binding of each compound to UCH-L3 increased and was dependent on the concentration of the compound **6** (data not shown).

2.5. Predicted binding mode

Figure 5 shows the predicted binding modes of compounds **1**, **6**, and **7** to UCH-L3. Since chemical formulae of the three compounds are similar to each other, the predicted docked structures of these and UCH-L3 have similar binding modes. Two hydrogen bonds were observed between the docked ligand and two amino acid residues in the predicted compound **1**/UCH-L3 complex structure; the carbonyl group of compound **1** appears to form a hydrogen bond to the NH group of Ala11, and the pyrrole C=O appears to form a hydrogen bond to the hydroxyl group of Thr157. Three hydrogen bonds were predicted between the docked ligand and two amino acid residues in the compound **6**/UCH-L3 complex structure; the thiadiazole group of compound **6** appears to form a hydrogen bond to the NH group of Leu9, and

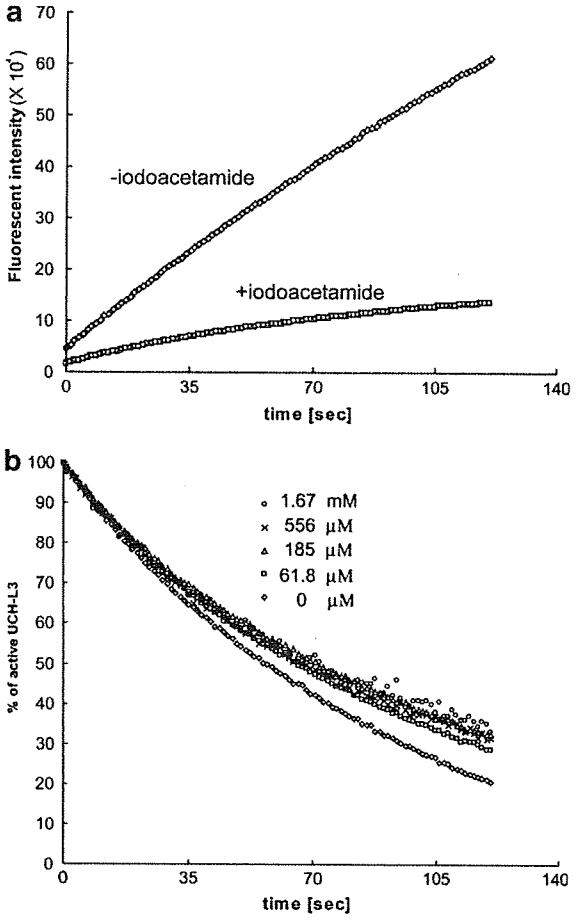

Figure 4. Competitive inhibition of compound **1**. (a) Kinetics of UCH-L3-catalyzed hydrolysis of Ub-AMC with or without iodoacetamide (108 mM). (b) Reaction progress curves normalized by final fluorescence intensity representing the ratio of active UCH-L3 (for calculations, see Section 4.9), in the presence of iodoacetamide (108 mM) and compound **1** (0 μM, 61.8 μM, 185 μM, 556 μM, and 1.67 mM).

the pyrrole hydroxyl group and pyrrole C=O appear to form a hydrogen bond to the NH group of Ala11. A hydrogen bond was observed between the docked ligand and the amino acid residues of UCH-L3 in the predicted compound **7**/UCH-L3 complex structure; the carbonyl group of compound **7** appears to form a hydrogen bond to the NH group of Ala11. The predicted binding mode of compound **10**, as a non-binder, was analyzed. Four hydrogen bonds were observed between the docked ligand and the amino acid residues of UCH-L3 in the predicted compound **10**/UCH-L3 complex structure. The triazol group of compound **10** appears to form two hydrogen bonds to the hydroxyl group of Thr157, and the amino group of compound **10** appears to form a hydrogen bond to the CO group of Glu154, and to the CO group of Ser151. Although hydrogen bonds between actual inhibitors (compounds **1**, **6**, and **7**) and Ala11 were observed, compound **10**, a non-inhibitor, does not appear to form a hydrogen bond to Ala11. This hydrogen bond might be important for compounds to bind stably to the UCH-L3 active site.

2.6. Discussion; analysis of active compounds

By three-step virtual screening (DOCK, high-speed GOLD, and low-speed GOLD) of 32,799 chemicals, we identified 10 candidate chemicals that potentially inhibit UCH-L3 hydrolysis activity. We examined the actual inhibitory effects of the compounds on UCH-L3 hydrolysis activity by biochemical enzymatic assay and identified three compounds (compounds **1**, **6**, and **7**) as UCH-L3 inhibitors, with IC_{50} values of 100–150 μM. By comparing the structural formulae of the three compounds, we found that the 1,5-dihydro-2*H*-pyrrol-2-one group is likely to be important for inhibition of UCH-L3-hydrolysis activity (Fig. 6). Several common structural features can be drawn from these three chemicals (Fig. 6). First, the heteroaromatic pyrrole group is common to all three compounds. Second, each of the three compounds also contains pyridines and furoyls as heteroaromatic functional groups. Third, a carbon–oxygen double bond at position 2, a hydroxyl group at position 3, a carbonyl group at position 4, and a hydrogen atom at position 5 of the pyrrole ring are common to each compound. Fourth, a five- or six-membered cyclic group at positions 1, 4, and 5 is common to all three chemicals (Fig. 6). Furthermore, compounds **1** and **7** have two heteroaromatic groups: a pyridinyl group and a furoyl group.

The structural similarities of UCH-L3-binding chemicals have an influence on binding mode similarities. There are two main pockets in the substrate-binding site of UCH-L3: the first pocket (Pocket 1) is formed by Pro8, Glu10, and Thr157 and the second pocket (Pocket 2), the active site pocket, is formed by Asp167, Leu168, and Cys90. Docked orientations of compounds **1** and **7** are very similar, as positions 1 and 5 six-membered cyclic groups fit into each pocket. This suggests that two features among these similarities are likely to be important for stable binding to the active site: a pyrrole ring and two heteroaromatic groups, which fit into both pockets around the UCH-L3 substrate-binding site. The shape of Pocket 1 is different from that of UCH-L1,[24] another isoform of the UCH family (52% amino acid sequence identity).[25] Thus, modification of the chemical groups in Pocket 1 might be effective during drug design, to enhance specificity for UCH-L3 over UCH-L1.

Several lines of evidence indicate that UCH-L3 is associated with tumorigenesis and carcinogenesis. High-level expression and activity of UCH-L3 has been reported in multiple types of cancer cells. Expression of UCH-L3 mRNA is upregulated in breast tumors and UCH-L3 mRNA levels are associated with the histological grading of such tumors.[5] Moreover, it has been suggested that the activity of UCH-L3 is also upregulated in the majority of cervical carcinoma tissues, compared with adjacent normal tissues.[6] On the other hand, loss of UCH-L3 is known to induce cell death in knock-out studies. UCH-L3 is involved in the protection of programmed cell death in germ cells and photoreceptor cells in vivo.[7,8] Thus, the structural information of the

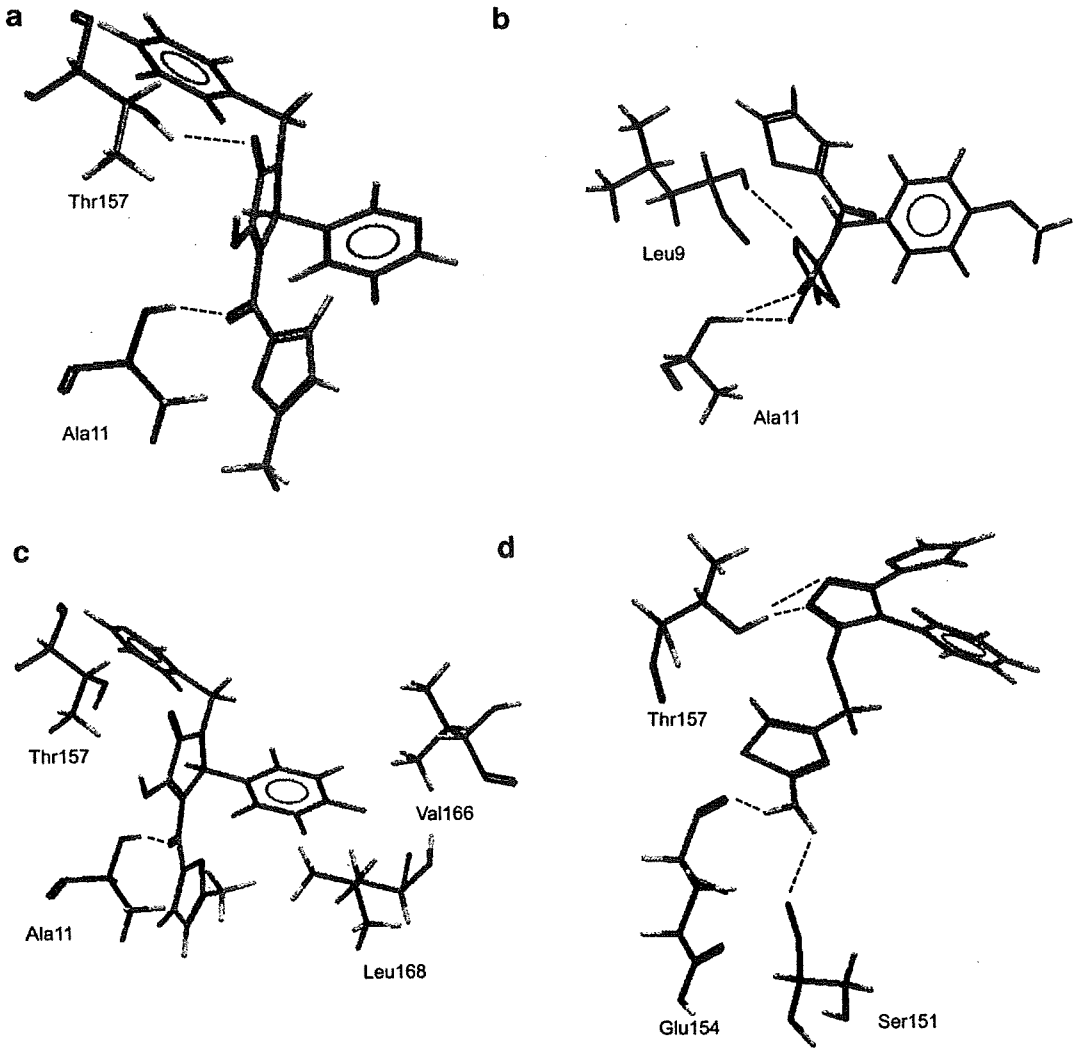

Figure 5. Illustration showing the molecular docking results. Docked orientation of (a) compound **1**, (b) compound **6**, (c) compound **7**, and (d) compound **10** in the UCH-L3 active site using GOLD and shown with interacting residues. Hydrogen bonds are shown by a dashed line. Oxygen atoms are shown in red, nitrogen atoms in blue, sulfur atoms in orange, fluorine atoms in yellow, and hydrogen atoms in gray. The enzyme carbons are shown in dark gray and those of the ligands in green.

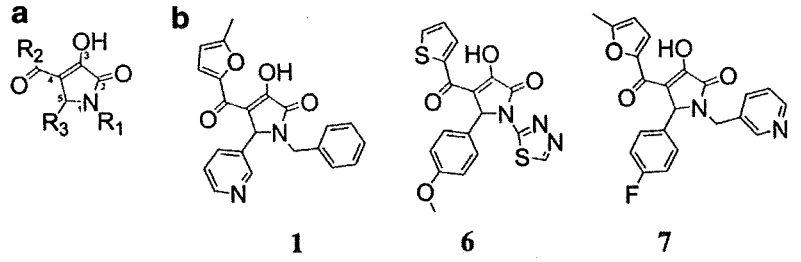

Figure 6. Structural similarities of the three compounds. (a) 1,5-Dihydro-2*H*-pyrrol-2-one group, the common basic skeleton, is shown in red. Position numbers of the pyrrole ring are shown as small characters. R_1–R_3 represent each functional group at positions 1, 4, and 5 of the pyrrole ring, respectively. (b) Structures of identified inhibitors: compounds **1**, **6**, and **7**.

UCH-L3 inhibitors we identified may be useful for future apoptosis-inducing anti-cancer drug development. UCH-L3 should be an important target for modulating cell apoptosis.

3. Conclusion

In this study, we employed three-step docking (DOCK, rough GOLD, and fine GOLD) and in vitro enzyme

assay methods, and identified three UCH-L3 inhibitors with IC_{50} values of 100–150 μM. These novel inhibitors have a dihydro-pyrrole group in common.

4. Experimental

4.1. Compound library

We used the ADME/Tox (absorption, distribution, metabolism, excretion, and toxicity) filtered virtual compound library (ChemBridge CNS-Set) which includes a collection of 32,799 chemical compounds.[18] All compounds satisfy Lipinski's Rule of five.

4.2. Protein preparation

Human UCH-L3 and ubiquitin vinylmethylester (Ub-VME) complex crystal structure data (PDB code; 1XD3) were obtained from Protein Data Bank (PDB).[17] Hydrogens were added to UCH-L3-ubiquitin complex using CVFF99 force field by Biopolymer module in Insight II 2000 suite (Accelrys, Inc., San Diego, CA). Energy was minimized by the Discover 3 module of the same suite with all heavy atoms restrained, except hydrogen, to relieve any short contacts. To use the UCH-L3 protein structure in the following docking simulations, the structures of UCH-L3 and Ub-VME complex were divided into their components.

4.3. Virtual screening

Virtual screening experiments were performed by UCSF DOCK 5.4.0[10] and GOLD 3.0.1 (CCDC, Cambridge, UK).[26] In the first screening by DOCK, the substrate-binding site was defined, by selecting ligand atom accessible spheres and describing molecular surfaces with the SPHERE_GENERATOR program in the DOCK suite. All spheres within 6 Å of root mean square deviation (RMSD) from every atom of the three C-terminal residues of energy-minimized ubiquitin were selected by the SPHERE_SELECTOR program in DOCK suite. A scoring function ($E_{int} = E_{vdw} + E_{elec}$) was used to estimate potential binding affinity. Following the first screening with rigid ligand conditions, 1780 compounds with binding energy scores of less than −30 kcal/mol were selected for a second screening by GOLD.

Using GOLD, the 1780 compounds were screened with 7–8 times speed-up settings; that is, the pre-defined genetic algorithm (GA) parameter settings to achieve calculation speed-up. The top-ranked 100 compounds were determined, then screened by default settings; the GA parameter settings for a slower calculation with greater ligand flexibility, but with a more accurate prediction. Ligand flexibility was turned on in both the 7–8 times speed-up settings and the default settings. Protein side chain flexibility was not turned on in any settings. The virtual tripeptide structure composed of three C-terminal residues of the energy-minimized ubiquitin was set as the reference ligand to define the ligand-binding site. All protein atoms within 5 Å of each ligand atom were used for defining the binding site. The solvent-accessible surfaces of the docking region were restricted by a cavity detection algorithm.[27] As a result, the binding site was composed of 174 active atoms (automatically selected by GOLD software). A method for defining the binding site with tripeptide yielded the best score among other methods using shorter or longer C-terminal peptide sequences of ubiquitin (data not shown). Ten docking solutions for each docked molecule were scored and the top three were saved for post-screening evaluations. Potential hydrogen bonds and van der Waals contacts were identified using Silver 1.0 (CCDC, Cambridge, UK).[28] Ligands predicted to be tight-binders by both DOCK and GOLD were applied to further in vitro experimental validation. All calculations were performed on seven Linux or Cygwin 2–3 GHz/Pentium IV CPU personal computers.

4.4. Statistical analysis

All statistical analysis was performed by GraphPad Prism 4 (GraphPad Software, Inc., San Diego, CA).[29]

4.5. Reagents

Human recombinant UCH-L3, ubiquitin-7-amido-4-methylcoumarin (Ub-AMC), and ubiquitin-aldehyde (Ub-H) were purchased from Boston Biochem, Inc. (Cambridge, MA). 4,5,6,7-Tetrachloroindan-1,3-dione (TCI) was purchased from Fisher Scientific International Inc. (Hampton, NH). Iodoacetamide was purchased from Sigma–Aldrich Corporation (St. Louis, MO). Compounds within ChemBridge CNS-Set (Supplier IDs given in parentheses) are as follows: compound **1**: 1-benzyl-3-hydroxy-4-(5-methyl-2-furoyl)-5-(3-pyridinyl)-1,5-dihydro-2*H*-pyrrol-2-one (7504601); compound **2**: 3-[4-methyl-5-({[3-(2-thienyl)-1,2,4-oxadiazol-5-yl]methyl}thio)-4*H*-1, 2,4-triazol-3-yl]-1*H*-indole (7950509); compound **3**: *N*-{4-[1-(2-furoyl)-5-(2-furyl)-4,5-dihydro-1*H*-pyrazol-3-yl]phenyl}methanesulfonamide (7977303); compound **4**: N^1-cyclopropyl-N^2-(4-methoxyphenyl)-N^2-[(4- methylphenyl)sulfonyl]glycinamide (6382507); compound **5**: *N*-{3-[1-acetyl-5-(2-thienyl)-4,5-dihydro-1*H*-pyrazol-3-yl]phenyl}ethanesulfonamide (7909542); compound **6**: 3-hydroxy-5-(4-methoxyphenyl)-1-(1,3,4-thiadiazol-2-yl)-4-(2-thienylcarbonyl)-1,5-dihydro-2*H*-pyrrol-2-one (6237842); compound **7**: 5-(4-fluorophenyl)-3-hydroxy-4-(5-methyl-2-furoyl)-1-(3-pyridinylmethyl)-1,5-dihydro-2*H*-pyrrol-2-one (6771097); compound **8**: N^1-cyclopropyl-N^2-[(4-methoxyphenyl)sulfonyl]-N^2-(4-methylphenyl)glycinamide (6699002); compound **9**: N^1-cyclopentyl-N^2-(3-methoxyphenyl)-N^2-(phenylsulfonyl)glycinamide (6187162); and compound **10**: 4-({[5-(2-furyl)-4-phenyl-4*H*-1,2,4-triazol-3-yl]thio}methyl)-1,3-thiazol-2-amine (9012750) were purchased from ChemBridge Corporation (San Diego, CA).

4.6. Enzymatic assay

UCH-L3 activity was assayed using modification of a technique described in previous studies.[22,30] The enzyme

reactions were carried out at a final volume of 205 μl on Costar 96-well black assay plates (part number 3915, Corning Inc., Corning, NY). Then, 5 μl of solution containing each compound (100% DMSO), or 5 μl of 100% DMSO as a negative control, was added to 100 μl of enzyme buffer solution (50 pM of UCH-L3, 20 mM Hepes [pH 7.8], 0.5 mM EDTA, 5 mM dithiothreitol [DTT], and 0.1 mg/ml ovalbumin) in each well. The solution was incubated for 30 min at room temperature. To start the enzyme reaction, 100 μl of substrate buffer solution (82 nM of ubiquitin-AMC, 20 mM Hepes [pH 7.8], 0.5 mM EDTA, 5 mM DTT, and 0.1 mg/ml ovalbumin) was added to each well. AMC fluorescence (excitation wavelength: 355 nm, emission wavelength: 460 nm) was subsequently measured 40 times every 3 s with a Wallac 1420 multi-label counter (Perkin-Elmer, Wellesley, MA).

4.7. K_m determination

Fifty microliters of enzyme buffer solution was added to each plate well. The solution was incubated for 30 min at room temperature. To start the enzyme reaction, 50 μl of substrate buffer solution (23.1, 46.3, 92.5, 185, 370, and 740 nM of ubiquitin-AMC; the concentrations of other components were as described previously) was added to each well. Fluorescence of AMC was measured 40 times every 3 s with the Wallac multi-label counter. Initial velocities (from 0 to 30 s) were used for K_m determination, using GraphPad Prism 4 software.[29]

4.8. Experimental IC_{50} determination

Five microliters of solution containing each compound (0.412 μM, 1.23, 3.70, 11.1, 20, 33.3, 50, 100, 300, and 700–850 μM) or 5 μl of 100% DMSO (as a negative control) diluted in 100 μl of enzyme buffer solution was added to each plate well. This solution was incubated for 30 min at room temperature. To start the enzyme reaction, 100 μl of substrate buffer solution was added to each well. Fluorescence of AMC was measured 40 times every 3 s with the Wallac multi-label counter. Initial velocities (from 0 to 30 s) were used for IC_{50} determination, using GraphPad Prism 4 software.[29]

4.9. Active site binding experiment

Modification of a technique described in previous studies was used to determine whether or not the compounds bind to the active site.[22] Five microliters of solution containing compound **1** (0 μM, 61.8 μM, 185 μM, 556 μM, and 1.67 mM), or 5 μl of 100% DMSO (as a negative control) diluted in 80 μl of enzyme buffer solution (UCH-L3: 1 nM) was added to each plate well. This solution was incubated for 30 min at room temperature. To start the enzyme reaction, 80 μl of substrate buffer solution (Ub-AMC: 1 μM) was added to each well, followed within 2 s by addition of 40 μl of iodoacetamide (108 mM) or water as a negative control. Fluorescence of AMC was measured 100 times every second using the Wallac multi-label counter. The percentage of active site survival $[(F_{saturated} - F_t)/(F_{saturated} - F_{t=0}) \times 100]$ was calculated.

Acknowledgments

This work was supported by Grants-in-Aid for Scientific Research from the Ministry of Health, Labour and Welfare of Japan, Grants-in-Aid for Scientific Research from the Ministry of Education, Culture, Sports, Science and Technology of Japan, a grant from the Program for Promotion of Fundamental Studies in Health Sciences of the National Institute of Biomedical Innovation, a grant from Japan Science and Technology Cooperation, and a grant from New Energy and Industrial Technology Development Organization. We thank Takashi Kaburagi for demonstrating how to set up the DOCK software.

References and notes

1. Ciechanover, A.; Schwartz, A. L. *Proc. Natl. Acad. Sci. U.S.A.* **1998**, *95*, 2727–2730.
2. Pickart, C. M.; Rose, I. A. *J. Biol. Chem.* **1985**, *260*, 7903–7910.
3. Waldmeier, P.; Bozyczko-Coyne, D.; Williams, M.; Vaught, J. L. *Biochem. Pharmacol.* **2006**, *72*, 1197–1206.
4. Aktas, O.; Waiczies, S.; Zipp, F. *J. Neuroimmunol.* **2007**, *184*, 17–26.
5. Miyoshi, Y.; Nakayama, S.; Torikoshi, Y.; Tanaka, S.; Ishihara, H.; Taguchi, T.; Tamaki, Y.; Noguchi, S. *Cancer Sci.* **2006**, *97*, 523–529.
6. Rolen, U.; Kobzeva, V.; Gasparjan, N.; Ovaa, H.; Winberg, G.; Kisseljov, F.; Masucci, M. G. *Mol. Carcinog.* **2006**, *45*, 260–269.
7. Kwon, J.; Wang, Y. L.; Setsuie, R.; Sekiguchi, S.; Sato, Y.; Sakurai, M.; Noda, M.; Aoki, S.; Yoshikawa, Y.; Wada, K. *Am. J. Pathol.* **2004**, *165*, 1367–1374.
8. Sano, Y.; Furuta, A.; Setsuie, R.; Kikuchi, H.; Wang, Y. L.; Sakurai, M.; Kwon, J.; Noda, M.; Wada, K. *Am. J. Pathol.* **2006**, *169*, 132–141.
9. Kuntz, I. D.; Blaney, J. M.; Oatley, S. J.; Langridge, R.; Ferrin, T. E. *J. Mol. Biol.* **1982**, *161*, 269–288.
10. Ewing, T. J.; Makino, S.; Skillman, A. G.; Kuntz, I. D. *J. Comput. Aided Mol. Des.* **2001**, *15*, 411–428.
11. FlexX, BioSolveIT GmbH, Sankt Augustin, Germany, <http://www.biosolveit.de/>.
12. Peng, H.; Huang, N.; Qi, J.; Xie, P.; Xu, C.; Wang, J.; Yang, C. *Bioorg. Med. Chem. Lett.* **2003**, *13*, 3693–3699.
13. McNally, V. A.; Gbaj, A.; Douglas, K. T.; Stratford, I. J.; Jaffar, M.; Freeman, S.; Bryce, R. A. *Bioorg. Med. Chem. Lett.* **2003**, *13*, 3705–3709.
14. Olsen, L.; Jost, S.; Adolph, H. W.; Pettersson, I.; Hemmingsen, L.; Jorgensen, F. S. *Bioorg. Med. Chem.* **2006**, *14*, 2627–2635.
15. Miteva, M. A.; Lee, W. H.; Montes, M. O.; Villoutreix, B. O. *J. Med. Chem.* **2005**, *48*, 6012–6022.
16. Johnston, S. C.; Larsen, C. N.; Cook, W. J.; Wilkinson, K. D.; Hill, C. P. *EMBO J.* **1997**, *16*, 3787–3796.
17. Misaghi, S.; Galardy, P. J.; Meester, W. J.; Ovaa, H.; Ploegh, H. L.; Gaudet, R. *J. Biol. Chem.* **2005**, *280*, 1512–1520.
18. RPBS, Paris, France, <http://bioserv.rpbs.jussieu.fr/RPBS/cgi-bin/Ressource.cgi?chzn_lg=an&chzn_rsrc=Collections/>.
19. GOLD User Guide, 16.2.1, CCDC, Cambridge, UK, <http://www.ccdc.cam.ac.uk/support/documentation/gold/3_1/gold31.pdf/>.
20. Dang, L. C.; Melandri, F. D.; Stein, R. L. *Biochemistry* **1998**, *37*, 1868–1879.

21. Mason, D. E.; Ek, J.; Peters, E. C.; Harris, J. L. *Biochemistry* **2004**, *43*, 6535–6544.
22. Liu, Y.; Lashuel, H. A.; Choi, S.; Xing, X.; Case, A.; Ni, J.; Yeh, L. A.; Cuny, G. D.; Stein, R. L.; Lansbury, P. T., Jr. *Chem. Biol.* **2003**, *10*, 837–846.
23. Stenlund, P.; Frostell-Karlsson, A.; Karlsson, O. P. *Anal. Biochem.* **2006**, *353*, 217–225.
24. Das, C.; Hoang, Q. Q.; Kreinbring, C. A.; Luchansky, S. J.; Meray, R. K.; Ray, S. S.; Lansbury, P. T.; Ringe, D.; Petsko, G. A. *Proc. Natl. Acad. Sci. U.S.A.* **2006**, *103*, 4675–4680.
25. Kurihara, L. J.; Semenova, E.; Levorse, J. M.; Tilghman, S. M. *Mol. Cell. Biol.* **2000**, *20*, 2498–2504.
26. Jones, G.; Willett, P.; Glen, R. C.; Leach, A. R.; Taylor, R. *J. Mol. Biol.* **1997**, *267*, 727–748.
27. Hendlich, M.; Rippmann, F.; Barnickel, G. *J. Mol. Graph. Model.* **1997**, *15*, 359–363.
28. Silver, CCDC, Cambridge, UK, <http://www.ccdc.cam.ac.uk/>.
29. GraphPad Prism 4, GraphPad Software, San Diego, CA, <http://www.graphpad.com/www/about.htm/>.
30. Nishikawa, K.; Li, H.; Kawamura, R.; Osaka, H.; Wang, Y. L.; Hara, Y.; Hirokawa, T.; Manago, Y.; Amano, T.; Noda, M.; Aoki, S.; Wada, K. *Biochem. Biophys. Res. Commun.* **2003**, *304*, 176–183.

Available online at www.sciencedirect.com
ScienceDirect
Biochemical and Biophysical Research Communications 355 (2007) 41–46
BBRC
www.elsevier.com/locate/ybbrc

Neuroligins 3 and 4X interact with syntrophin-γ2, and the interactions are affected by autism-related mutations

Hidekuni Yamakawa [a], Satoko Oyama [a], Hiroaki Mitsuhashi [a], Noboru Sasagawa [a], Shigeo Uchino [b], Shinichi Kohsaka [b], Shoichi Ishiura [a,*]

[a] *Department of Life Sciences, Graduate School of Arts and Sciences, University of Tokyo, Tokyo, 3-8-1 Komaba, Meguro-ku, 153-8902, Japan*
[b] *Department of Neurochemistry, National Institute of Neuroscience, Tokyo, 4-1-1 Ogawahigashi, Kodaira, 187-8502, Japan*

Received 4 January 2007
Available online 31 January 2007

Abstract

Recently, neuroligins (NLs)3 and 4X have received much attention as autism-related genes. Here, we identified syntrophin-γ2 (SNTG2) as a *de novo* binding partner of NL3. SNTG2 also bound to NL4X and NL4Y. Interestingly, the binding was influenced by autism-related mutations, implying that the impaired interaction between NLs and SNTG2 contributes to the etiology of autism.

Keywords: Autism; Neuroligin; Scaffolding protein; Syntrophin

Neuroligin (NL) is a neural cell adhesion molecule, which was identified as a ligand for β-neurexin [1]. Rodents possess three NLs, all of which interact with β-neurexin, while humans have five NLs. The trans-synaptic interaction between NL and β-neurexin strongly induces both pre- and postsynaptic maturation [2–4]. Interestingly, mutations of human *NL3* and *NL4X* are implicated in autism and mental retardation [5–9]. Autism is characterized by impaired reciprocal social interaction and communication and restricted, stereotyped patterns of interests and activities. Here, we investigated the *de novo* binding partners of NL3 using yeast two-hybrid screening, and found that syntrophin-γ2 (SNTG2) interacted with NL3, NL4X, and NL4Y, which are autism-related NL isoforms. Interestingly, the interactions between the NLs and SNTG2 are very noteworthy in terms of the etiology of autism because they are influenced by autism-related mutations.

Abbreviations: NL, neuroligin; PDZ, PSD/Dlg/ZO-1 homology; PSD, postsynaptic density; DIV, days *in vitro*; CNS, central nervous system.

* Corresponding author. Fax: +81 3 5454 6739.
E-mail address: cishiura@mail.ecc.u-tokyo.ac.jp (S. Ishiura).

0006-291X/$ - see front matter © 2007 Elsevier Inc. All rights reserved.
doi:10.1016/j.bbrc.2007.01.127

Materials and methods

Plasmid construction. Tag sequences and cDNA fragments were cloned into the pcDNA3.1 expression vector (Invitrogen, Carlsbad, CA) or in pECFP vector (Clontech, Palo Alto, CA) using conventional molecular biological techniques. The nucleotide sequences of the DNA inserts were confirmed using sequence analysis. The following NLin (intracellular region of human neuroligin) constructs were made: NL3in (731–848 aa), NL4Xin (698–816 aa), and NL4Yin (698–816 aa). For ΔPBM mutants, the C-terminus of NLs (six amino acids: HSTTRV) was deleted. For ΔTMD32 mutants, TMD32, the N-terminus 32 amino acids of NL3in, was deleted (see Fig. 1). The YFP-NLs contained each NL signal sequence followed by the enhanced yellow fluorescent protein (EYFP) and the mature N-terminus of each of the NLs inserted into pcDNA3.1 expression vector. The Myc × 6 tagged NLs also contained each NL signal sequence followed by Myc × 6 tags and the mature N-terminus of each of the NLs inserted into pcDNA3.1 expression vector. The full-length human syntrophin-γ2 (NCBI Accession No. NP_061841, hSNTG2) was inserted into the revised pACT2 vector to express the GAL4AD-fusion proteins in the yeast two-hybrid system. The FLAG-tagged SNTG2 contained three FLAG tags followed by the N-terminus of SNTG2. The Myc-tagged SNTG2 contained SNTG2 followed by six Myc tags.

Antibodies. We purchased the following rabbit polyclonal antibodies: anti-GFP (Molecular Probes, Eugene, OR) and anti-FLAG (Sigma, St. Louis, MO). In addition, we obtained the following mouse monoclonal antibodies: anti-synaptophysin (Chemicon), anti-MAP2, anti-FLAG M2 (Sigma), anti-Myc, and anti-V5 (Invitrogen).

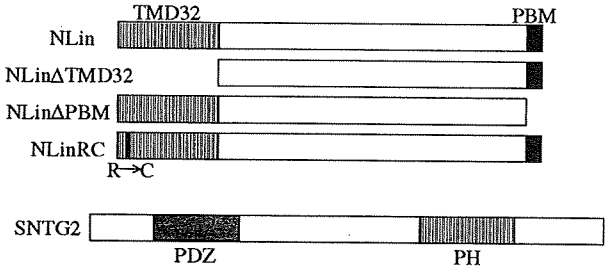

Fig. 1. Schematic depiction of the constructs of NLs and SNTG2. Vertical-striped, black, gray, and horizontal-striped rectangles show the TMD32 domain, PDZ binding motif (PBM), PDZ domain, and PH domain, respectively.

Western blotting. Samples were run on 7.5% SDS–polyacrylamide gels and transferred to PVDF membranes (Immobilon-P; Millipore). The membranes were blocked with 5% skim milk in TPBS (PBS with 0.05% Tween®20) for 1 h at room temperature and then incubated for 1–2 h with primary antibodies in TPBS. After washing, the membranes were incubated for 1 h with HRP-conjugated secondary antibodies. The immunoreactive bands were visualized using ECL.

Yeast two-hybrid screening. Yeast two-hybrid assays were performed using the MATCHMAKER GAL4 Two-Hybrid System (Clontech). The cDNA fragments encoding the intracellular region of human NL3 (711–828 aa, NCBI Accession No. NP_061850, hNL3in) were amplified by PCR and cloned into the *Eco*RI and *Bam*HI restriction sites of the pAS2-1C vector to serve as bait in the yeast two-hybrid screening. The pAS2-1C vector is the pAS2-1 vector (Clontech) revised as a single-copy plasmid in yeasts. The nucleotide sequences of the DNA inserts were confirmed by sequence analysis to verify that the inserts did not contain mutations. The human fetal brain MATCHMAKER cDNA library in the pACT2 vector (Clontech) served as prey in the yeast two-hybrid screening. The inserts were expressed as fusion proteins with the DNA-binding and DNA-activating domains of GAL4. Details of the other constructs used in the yeast two-hybrid assays are presented in Fig. 1.

Yeast was transformed using the lithium acetate method with 30% polyethylene glycol 4000. In screening the NL3in-binding partners, 5 μg cDNA library per plate were introduced into transformants of NL3in in pAS2-1C. Transformants were selected on −LWHA and −LWH + 3-AT plates, and then the surviving transformants were selected using the β-galactosidase assay. We screened more than 1×10^6 cells. The intensity of the interactions between NLs and SNTG2 was examined using the 3-AT assay.

Immunoprecipitation. COS-7 cells were transfected with Myc-tagged constructs of NL and FLAG-tagged constructs of SNTG2 using FuGENE 6 (Roche, Basel, Switzerland). Cells from two 10-cm plates were homogenized in 500 μl of Lysis Buffer (50 mM Tris/HCl [pH 8.0] containing 200 mM NaCl, 5 mM DTT, 1 mM EDTA, 1% (w/v) Triton X-100, and protease inhibitor cocktail). Then, the lysates were centrifuged at 100,000*g* for 15 min at 4 °C. The supernatant was precleared with protein G Sepharose 4 fast flow beads (Amersham Biosciences, Piscataway, NJ) for 1 h and then incubated with 1 μl of anti-FLAG M2 antibody fixed on 15 μl beads. After the beads were washed five times with homogenization buffer, the precipitates were analyzed using SDS–PAGE and immunoblotted with either anti-Myc or anti-FLAG antibody.

Immunocytochemistry and image analysis. Cortical neurons and COS-7 cells were fixed with PBS containing 2% or 4% (w/v) paraformaldehyde for 15 min, and permeabilized with 0.1% (w/v) Triton X-100 in PBS for 15 min. After the buffer was exchanged for 3% (w/v) BSA in PBS, the cells were incubated with the first antibody in 3% BSA in PBS for 1 h, washed with PBS, and then incubated with the second antibody in 3% BSA in PBS for 1 h. After washing with PBS, the samples were embedded in Mowiol (Calbiochem, La Jolla, CA). When only the cell surface was stained, the cells were incubated with the first antibody in PBS for 20 min, washed with PBS, and incubated with the second antibody for 20 min before washing and fixing. Z-stacks of four to 10 images were acquired on a Zeiss LSM510 meta laser scanning confocal microscope (Carl Zeiss, Jena, Germany). Brightest point projections of the Z-stacks were used for image analysis.

Neuronal cultures and transfection. Neurons were dissociated from the cerebral cortices of E18 rats and cultured at a density of 5×10^4 cells/cm^2 in Neurobasal medium with 2% B27 supplement (Invitrogen), 200 mM L-glutamine, and 10 mM L-glutamate at 37 °C under a controlled atmosphere containing 10% CO_2. After 7 or 11 days *in vitro*, the neurons were transfected with 1 μg DNA per well in 12-well plates using Lipofectamine™ 2000 (Invitrogen) according to the manufacturer's directions.

Results

Library screening identified syntrophin-γ2 as an NL3in-binding protein

While some reports have implied that GABA synapses are somehow involved in the pathology of autism [10,11], no scaffolding protein which exclusively localizes in the inhibitory synapse has been identified as a binding partner of NL3, which is thought to be strongly tied to autism [5,6]. NLs have been reported to be associated with both excitatory and inhibitory synapses. Therefore, we hypothesized that some unknown scaffolding proteins were associated with NL in inhibitory synapses, and that the interactions were involved in the pathology of autism. To identify these unknown scaffolding proteins, we performed yeast two-hybrid screening using the intracellular region of NL3 (NL3in) as bait to screen a human fetal brain cDNA library. Syntrophin-γ2 (SNTG2) was identified as a putative candidate. We confirmed the authenticity of the clone by transforming it back into yeast with NL3in.

Moreover, to determine the SNTG2-binding regions in NLs, we performed the HIS3 assay using various constructs (Fig. 1) that express mutant NL-fusion proteins in yeasts (Table 1). We examined the binding of NL3, 4X, and 4Y to SNTG2 in yeasts. All of the autism-related

Table 1
Results of the HIS3 assay of the NL mutants

Construct	HIS3 assay
Vector (DBD)	+
NL3in	++++++
NL3inΔPBM	+
NL3inR737C	+++
NL3inR737CΔPBM	+
NL3inΔTMD32	+++
NL4Xin	++++++
NL4XinΔPBM	+
NL4XinR704C	+++
NL4XinR704CΔPBM	+
NL4Yin	++++
NL4YinR704C	+++

We examined the strength of the interactions between NL or NL mutants and SNTG2 using the HIS3 assay. Since the HIS3 gene product, which is required for cell growth on plates lacking histidine, is competitively inhibited by 3-AT, the concentration of 3-AT at which yeast transformants can grow represents the activity of HIS3. Therefore, it reflects the strength of the interaction. Six, five, four, three, two, and one plus (+) indicate 3-AT concentrations of 20, 15, 10, 5, 1, and 0 mM, respectively.

NLs bound to SNTG2. The deletion of the PDZ binding motif (PBM) from NL3, 4X, and 4Y disrupted this binding to SNTG2. Notably, the introduction of an R→C point mutation, an autism-related mutation [9], weakened the binding. Similarly, the deletion of TMD32, the region including the autism-related mutation, also weakened the binding of NL3 to SNTG2. These results suggest that the binding of NLs to SNTG2 depends mainly on PBM and is stabilized by TMD32.

NLs bound to SNTG2 in COS-7 cells

Next, we confirmed that NLs would bind to SNTG2 in COS-7 cells using immunoprecipitation. Myc-NL3 and Myc-NL4X were co-immunoprecipitated with SNTG2 when FLAG-SNTG2 was immunoprecipitated using anti-FLAG antibody, whereas Myc-NL3 and Myc-NL4X were not immunoprecipitated by normal IgG, suggesting that NL3 and NL4X specifically interacted with SNTG2 (Fig. 2). In addition, Myc-NL4Y bound to FLAG-SNTG2 in COS-7 cells (data not shown).

We also examined the binding of NL mutants to SNTG2 in COS-7 cells. As with the HIS3 assay, the deletion of PBM in NL drastically weakened the binding to SNTG2 (Fig. 3A), indicating that the interaction between SNTG2 and NL in mammalian cells is mostly dependent on PBM. In contrast, the autism-related R704C mutation in NL4X did not seem to alter the binding (Fig. 3B). This result seems to be inconsistent with HIS3 assay. However, we suppose that we couldn't detect the effect of the autism-related R704C on the interaction between NL4X and SNTG2 because immunoprecipitation is not sensitive enough to detect minute differences of affinity. We also examined the regions of SNTG2 involved in its binding to NLs in COS-7 cells. The deletion of either the N- or C-terminal half of SNTG2 dramatically weakened the binding to NL3 and NL4X (Fig. 3C), suggesting that both the N-terminal part, including the PDZ domain, and the C-terminal half of SNTG2 are involved in the binding to NL.

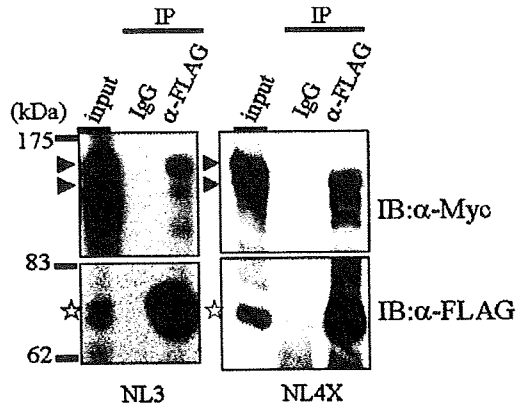

Fig. 2. The binding between SNTG2 and NLs in COS-7 cells. Myc-NLs were co-immunoprecipitated with FLAG-SNTG2 using anti-FLAG M2 antibody in Lysis buffer. Immunoprecipitation using normal mouse IgG was the negative control. Arrowheads and stars indicate Myc-NLs and FLAG-SNTG2, respectively. Both arrowheads may denote the posttranslational modification of NLs.

NLs partially colocalize with SNTG2 in both COS-7 cells and rat cortical neurons

To determine whether NL and SNTG2 colocalize because of their interaction, we immunostained COS-7 cells expressing YFP-NLs and SNTG2-myc. When YFP-NL3 or YFP-NL4X was expressed after transfecting COS-7 cells, it formed a small cluster on the cell surface (Fig. 4A). When SNTG2-myc was also expressed, it partially colocalized with YFP-NL (Fig. 4B); however, SNTG2-myc did not alter the localization of YFP-NL on the cell surface substantially, and vice versa.

Next, we examined the localization of exogenous NL3 and SNTG2 in rat cortical neurons at DIV9. When YFP-NL3 was expressed by transfection, YFP-NL3 formed small clusters on the surface of soma and dendrites, just like endogenous NL3 (Fig. 4C). Clusters of YFP-NL3 often colocalized with SNTG2-myc when neurons were doubly transfected, supporting the idea that NL3 is associated with SNTG2 in neurons and that SNTG2 functions as a scaffolding protein.

Discussion

This study revealed functional differences among NLs, which were related to binding to syntrophin-γ2 (SNTG2). Here, SNTG2 was identified as a *de novo* binding partner of autism-related NLs using yeast two-hybrid screening. SNTG2 is a member of the syntrophin family, whose members have a PDZ domain near the N-terminus and a PH domain near the C-terminus. Syntrophins play a key role as scaffolding proteins in both neuromuscular junctions and the CNS, where they interact with dystrophin and dystrobrevin [12]. Interestingly, the CNS syntrophins have been reported to localize exclusively in the inhibitory postsynaptic regions by binding to dystrophin and dystrobrevin [13,14]. Therefore, SNTG2 may be an unknown NL-binding scaffolding protein in inhibitory synapses.

The interaction between SNTG2 and NLs was mainly dependent on the PBM-PDZ interaction because it was disrupted by the deletion of PBM in NLs (Table 1 and Fig. 3A). Meanwhile, the binding of NLs to SNTG2 was influenced by factors other than the PBM-PDZ interaction, involving TMD32 in NLs and the region including PH in SNTG2 (Table 1 and Fig. 3B and C). Since deletion of the PBM disrupted the binding, we postulated that these non-PBM-PDZ factors somehow stabilize the PBM-PDZ core interaction. In particular, the effect of TMD32 on binding is interesting because it was previously reported to be necessary for the proper localization of NL1 [15]. In addition, TMD32 is variable

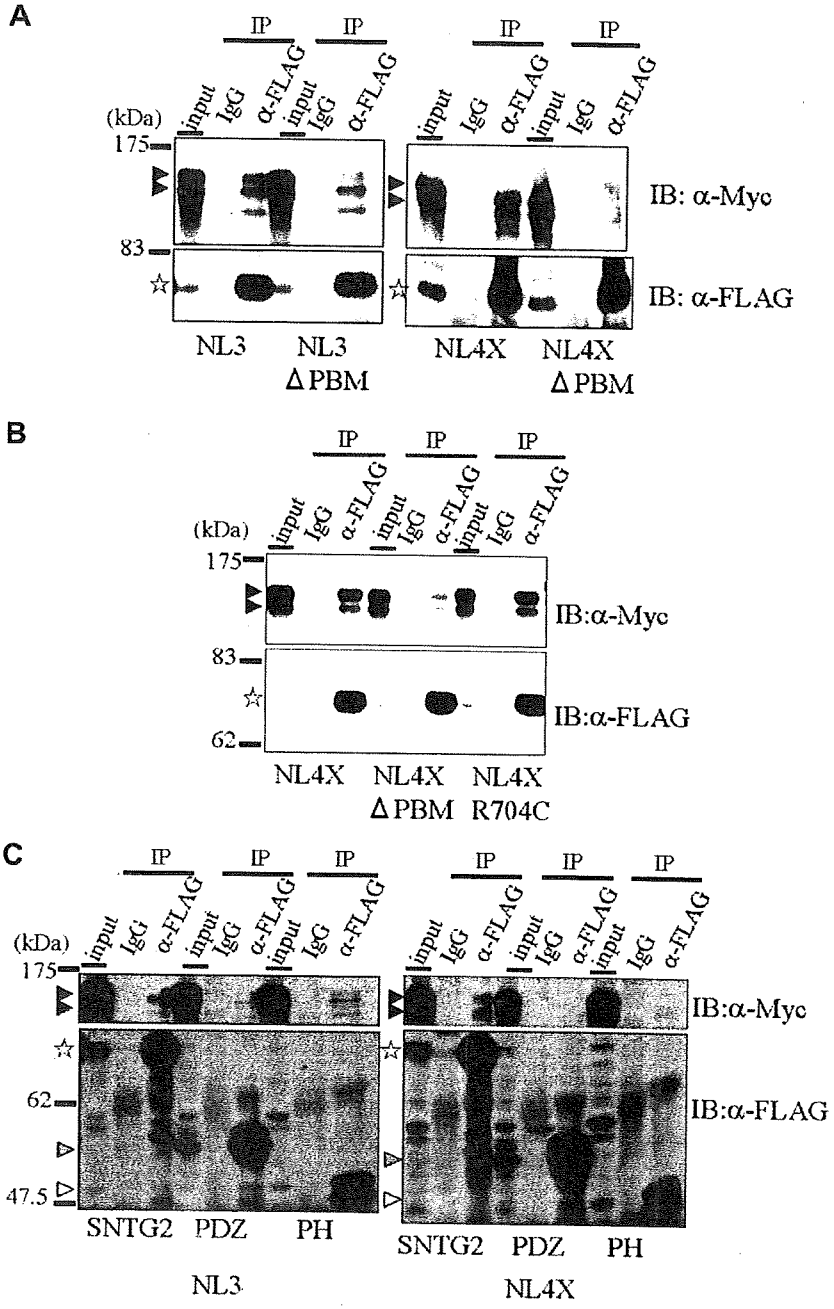

Fig. 3. (A) Effects of the deletion of PBM in NLs on the binding between SNTG2 and NLs in COS-7 cells. Various Myc-tagged NLs were co-immunoprecipitated with FLAG-SNTG2 in Lysis buffer. The deletion of PBM in NLs weakened the binding of NLs to SNTG2. Arrowheads and stars indicate Myc-NLs and FLAG-SNTG2, respectively. (B) The effect of R704C in NL4X, the autism-related mutation, on the binding to SNTG2 in COS-7 cells. Various Myc-tagged NL4Xs were co-immunoprecipitated with FLAG-SNTG2 in Lysis buffer. Under these conditions, the effect of the R704C mutation on the binding to SNTG2 was not detected. (C) The role of PDZ or the PH domain of SNTG2 in binding to NL. Whenever the regions containing the PDZ or PH domain were deleted, binding to NL was weakened. Therefore, both these regions might be involved in the interaction between NL and SNTG2. Black, gray, and white arrowheads and the star indicate Myc-NLs, the FLAG-tagged region containing the PDZ domain, the FLAG-tagged region containing the PH domain of SNT2G2, and the FLAG-tagged full-length SNTG, respectively.

in comparison with other parts of NL. These findings led us to hypothesize that due to the diversity of TMD32, NLs are functionally different from each other and the sequence of TMD32 for each NL determines whether the NL localizes in the inhibitory synapse. In this experiment, we could not examine the interaction between SNTG2 and NL2, which has been reported to localize in the inhibitory synapse exclusively. However, NL2 is

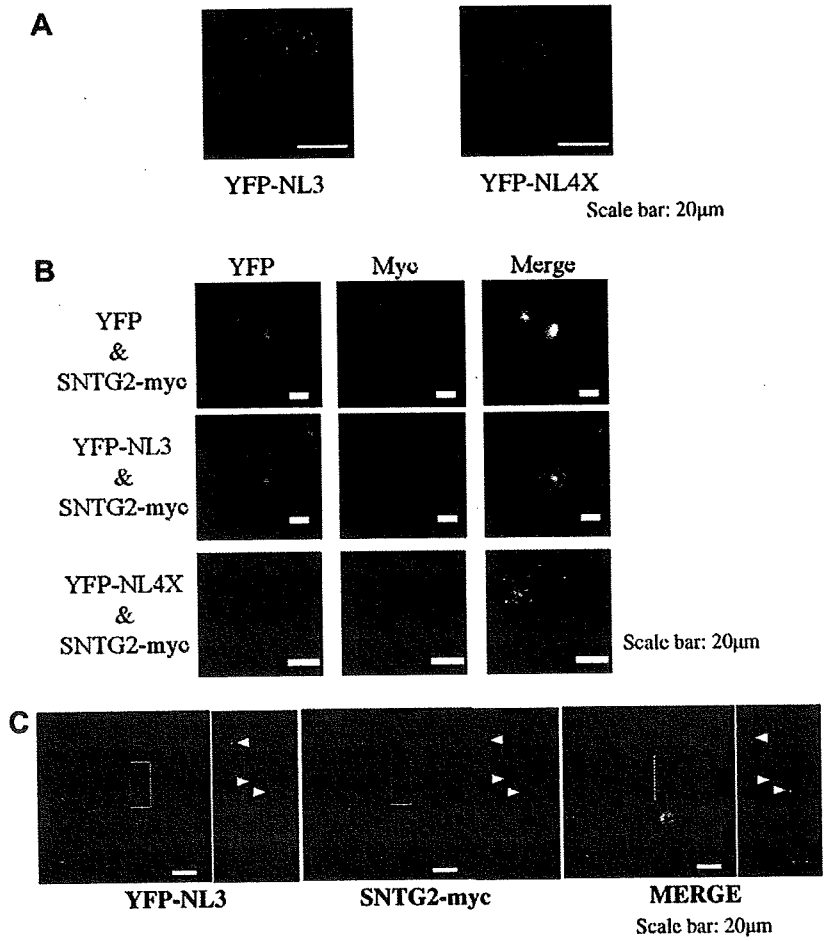

Fig. 4. (A) Localization of NL3 and NL4X on the surface of COS-7 cells. Only YFP-NL3 and YFP-NL4X on the cell-surface were immunostained using anti-GFP antibody and the secondary antibody conjugated with Oregon Green 488 without membrane permeabilization. They were clustered on the cell surface. (B) Localization of NLs and SNTG2 in COS-7 cells. The upper panels are negative controls. YFP or YFP-NL of cell-surface, SNTG2-Myc and merged images are shown on the left, center, and right, respectively. Co-transfected YFP-NL and SNTG2-Myc partially colocalized. Scale bar, 20 μm. (C) Localization of NL3, NL4X, and SNTG2 in rat cortical neurons. Neurons were transfected with YFP-NL3 and SNTG2-Myc at DIV7 using Lipofectamine 2000. After a 48-h incubation, the neurons were fixed, immunostained, and observed under confocal microscopy. The boxed area is enlarged in the bottom row. The clusters of YFP-NL3 of cell-surface sometimes colocalized with the cluster of SNTG2-Myc (arrowhead). Scale bar, 20 μm.

expected to bind to SNTG2 much stronger than any other NL, considering that both NL2 and SNTG2 dominantly localize in the inhibitory synapse [13,14,16]. The interaction will be determined in future.

Recently, some reports have suggested that the balance between excitatory and inhibitory synapses is disrupted in patients with autism [17,18]. A postmortem analysis of the brains of subjects with autism indicated that glutamic acid decarboxylase (GAD) was reduced in the autistic parietal and cerebellar cortices [11], suggesting that the impairment of GABAergic synaptic transmission causes autism. Meanwhile, the binding of NLs to SNTG2, a putative inhibitory-synaptic scaffolding protein, were affected by autism-related mutations in *NLs* in our experiments. Totally, the interactions between NLs and SNTG2 at the inhibitory synapse may be deeply involved in the etiology of autism. In future, screening autistic individuals for *SNTG2* mutations may elucidate the association between autism and the binding of SNTG2 to NLs.

References

[1] K. Ichtchenko, Y. Hata, T. Nguyen, B. Ullrich, M. Missler, C. Moomaw, T.C. Sudhof, Neuroligin 1: a splice site-specific ligand for beta-neurexins, Cell 81 (1995) 435–443.
[2] E.R. Graf, X. Zhang, S.X. Jin, M.W. Linhoff, A.M. Craig, Neurexins induce differentiation of GABA and glutamate postsynaptic specializations via neuroligins, Cell 119 (2004) 1013–1026.
[3] C. Dean, F.G. Scholl, J. Choih, S. DeMaria, J. Berger, E. Isacoff, P. Scheiffele, Neurexin mediates the assembly of presynaptic terminals, Nat. Neurosci. 6 (2003) 708–716.

[4] P. Scheiffele, J. Fan, J. Choih, R. Fetter, T. Serafini, Neuroligin expressed in nonneuronal cells triggers presynaptic development in contacting axons, Cell 101 (2000) 657–669.
[5] S. Jamain, H. Quach, C. Betancur, M. Rastam, C. Colineaux, I.C. Gillberg, H. Soderstrom, B. Giros, M. Leboyer, C. Gillberg, et al., Mutations of the X-linked genes encoding neuroligins NLGN3 and NLGN4 are associated with autism, Nat. Genet. 34 (2003) 27–29.
[6] B. Chih, S.K. Afridi, L. Clark, P. Scheiffele, Disorder-associated mutations lead to functional inactivation of neuroligins, Hum. Mol. Genet. 13 (2004) 1471–1477.
[7] D. Comoletti, A. De Jaco, L.L. Jennings, R.E. Flynn, G. Gaietta, I. Tsigelny, M.H. Ellisman, P. Taylor, The Arg451Cys-neuroligin-3 mutation associated with autism reveals a defect in protein processing, J. Neurosci. 24 (2004) 4889–4893.
[8] F. Laumonnier, F. Bonnet-Brilhault, M. Gomot, R. Blanc, A. David, M.P. Moizard, M. Raynaud, N. Ronce, E. Lemonnier, P. Calvas, et al., X-linked mental retardation and autism are associated with a mutation in the NLGN4 gene, a member of the neuroligin family, Am. J. Hum. Genet. 74 (2004) 552–557.
[9] J. Yan, G. Oliveira, A. Coutinho, C. Yang, J. Feng, C. Katz, J. Sram, A. Bockholt, I.R. Jones, N. Craddock, et al., Analysis of the neuroligin 3 and 4 genes in autism and other neuropsychiatric patients, Mol. Psychiatry 10 (2005) 329–332.
[10] M.M. Menold, Y. Shao, C.M. Wolpert, S.L. Donnelly, K.L. Raiford, E.R. Martin, S.A. Ravan, R.K. Abramson, H.H. Wright, G.R. Delong, et al., Association analysis of chromosome 15 gabaa receptor subunit genes in autistic disorder, J. Neurogenet. 15 (2001) 245–259.
[11] S.H. Fatemi, A.R. Halt, J.M. Stary, R. Kanodia, S.C. Schulz, G.R. Realmuto, Glutamic acid decarboxylase 65 and 67 kDa proteins are reduced in autistic parietal and cerebellar cortices, Biol. Psychiatry 52 (2002) 805–810.
[12] M.E. Adams, N. Kramarcy, T. Fukuda, A.G. Engel, R. Sealock, S.C. Froehner, Structural abnormalities at neuromuscular synapses lacking multiple syntrophin isoforms, J. Neurosci. 24 (2004) 10302–10309.
[13] G. Piluso, M. Mirabella, E. Ricci, A. Belsito, C. Abbondanza, S. Servidei, A.A. Puca, P. Tonali, G.A. Puca, V. Nigro, Gamma1- and gamma2-syntrophins, two novel dystrophin-binding proteins localized in neuronal cells, J. Biol. Chem. 275 (2000) 15851–15860.
[14] I. Brunig, A. Suter, I. Knuesel, B. Luscher, J.M. Fritschy, GABAergic terminals are required for postsynaptic clustering of dystrophin but not of GABA(A) receptors and gephyrin, J. Neurosci. 22 (2002) 4805–4813.
[15] T. Dresbach, A. Neeb, G. Meyer, E.D. Gundelfinger, N. Brose, Synaptic targeting of neuroligin is independent of neurexin and SAP90/PSD95 binding, Mol. Cell Neurosci. 27 (2004) 227–235.
[16] F. Varoqueaux, S. Jamain, N. Brose, Neuroligin 2 is exclusively localized to inhibitory synapses, Eur. J. Cell Biol. 83 (2004) 449–456.
[17] H. Cline, Synaptogenesis: a balancing act between excitation and inhibition, Curr. Biol. 15 (2005) R203–R205.
[18] N.K. Hussain, M. Sheng, Neuroscience. Making synapses: a balancing act, Science 307 (2005) 1207–1208.

American Journal of Medical Genetics Part A 143A:2804–2809 (2007)

Clinical Report

22q13 Microduplication in Two Patients With Common Clinical Manifestations: A Recognizable Syndrome?

Nobuhiko Okamoto,[1]* Takeo Kubota,[2] Yutaka Nakamura,[3] Ryusuke Murakami,[3] Toshiya Nishikubo,[4] Ichiro Tanaka,[4] Yukihiro Takahashi,[4] Shin Hayashi,[5] Issei Imoto,[5] Johji Inazawa,[5] Noboru Hosokai,[6] Shinichi Kohsaka,[7] and Shigeo Uchino[7]

[1]Department of Planning and Research, Osaka Medical Center and Research Institute for Maternal and Child Health, Osaka, Japan

[2]Department of Epigenetic Medicine, Interdisciplinary Graduate School of Medicine and Engineering, University of Yamanashi, Yamanashi, Japan

[3]Department of Pediatrics, Awaji Prefecutural Hopsital, Hyogo, Japan

[4]Department of Pediatrics, Nara Medical University, Nara, Japan

[5]Department of Molecular Cytogenetics, Medical Research Institute, Tokyo Medical and Dental University, Tokyo, Japan

[6]Research and Development Division, Mitsubishi Kagaku Bio-Clinical Laboratory, Tokyo, Japan

[7]Department of Neurochemistry, National Institute of Neuroscience, Kodaira, Tokyo, Japan

Received 15 September 2007; Accepted 10 February 2007

We report here on two unrelated patients (Patients 1 and 2) with a cryptic microduplication involving a 22q13 segment. Both patients manifested infantile hypotonia, developmental delay, and growth deficiency. In addition, an abnormal signal intensity area was detected in the frontal white matter of Patient 2 by brain MRI. Whole-genome microarray comparative genomic hybridization for Patient 1 and fluorescence in situ hybridization analysis with 22q-subtelomeric probes performed in both patients showed a submicroscopic 22q13 duplication that involved the *SHANK3* gene. The duplication in Patient 1 was de novo type, while that in Patient 2 was derived from a familial 17;22 translocation. The presence of common clinical manifestations in the two patients with the common duplicated region led to a conclusion that 22q terminal duplication is a recognizable clinical entity, that is, the 22q13 microduplication syndrome. © 2007 Wiley-Liss, Inc.

Key words: comparative genomic hybridization; the 22q13 microduplication syndrome; the 22q13 deletion syndrome; mental retardation; *SHANK3*

How to cite this article: Okamoto N, Kubota T, Nakamura Y, Murakami R, Nishikubo T, Tanaka I, Takahashi Y, Hayashi S, Imoto I, Inazawa J, Hosokai N, Kohsaka S, Uchino S. 2007. 22q13 microduplication in two patients with common clinical manifestations: A recognizable syndrome? Am J Med Genet Part A 143A:2804–2809.

INTRODUCTION

Terminal 22q13 deletion (the Phelan-McDermid syndrome, PMS) is one of diseases with submicroscopic telomere deletions [Phelan et al., 2001]. PMS is characterized by significant expressive language delay, mental retardation, hypotonia, minor craniofacial dysmorphisms (dolichocephaly, epicanthal folds, saddle nose with bulbous tip, abnormal ears, ptosis of eyelids), dysplastic toenails, increased tolerance to pain, relatively large hands and normal to advanced growth. Autistic features are often observed [Manning et al., 2004]. As there was a correlation between clinical features and deletion size, haploinsufficiency of the *SHANK3* (or *ProSAP2*) gene expressed in the cerebral cortex and cerebellum is thought as a major factor in the neurological symptoms of PMS [Bonaglia et al., 2001; Wilson et al., 2003; Koolen et al., 2005]. Recently, mutations in the

Grant sponsor: Ministry of Education, Culture, Sports, Science and Technology; Grant sponsor: Osaka Medical Center and Research Institute; Grant sponsor: Ministry of Health, Labor and Welfare of Japan.

*Correspondence to: Dr. Nobuhiko Okamoto, Department of Planning and Research, Osaka Medical Center and Research Institute for Maternal and Child Health, 840 Murodo-cho, Izumi, Osaka 594-1101, Japan.
E-mail: okamoto@osaka.email.ne.jp

DOI 10.1002/ajmg.a.31771